Volume 1 | Number 1 | Jan 2013 | Pages 1–100

Soft Matter

www.rsc.org/softmatter

ROYAL SOCIETY OF CHEMISTRY

ROYAL SOCIETY OF CHEMISTRY

www.rsc.org/softmatter

Effects of Nanoscopic-Confinement on Polymer Dynamics

Kiriaki Chrissopoulou[a] and Spiros H. Anastasiadis[a,b,∗]

[a] Institute of Electronic Structure and Laser, Foundation for Research and Technology -

Hellas, P. O. Box 1527, 711 10 Heraklion Crete, Greece

[b] Department of Chemistry, University of Crete, P. O. Box 2208, 710 03 Heraklion Crete,

Greece

Abstract

The static and dynamic behavior of polymers in confinement close to interfaces can be very different from that in the bulk. Among the various geometries, intercalated nanocomposites, in which polymer films of ~1 nm thickness reside between the parallel inorganic surfaces of layered silicates in a well-ordered multilayer, offer a unique avenue for the investigation of the effects of nanoconfinement on polymer structure and dynamics by utilizing conventional analytical techniques and macroscopic specimens. In this article, we provide a review of research activities mainly in our laboratory on polymer dynamics under severe confinement utilizing different polymer systems: polar and non-polar polymers were mixed with hydrophilic or organophilic silicates, respectively, whereas hyperbranched polymers were studied in an attempt to probe the effect of polymer-surface interactions by altering the number and the kind of functional groups in the periphery of the branched polymers. The polymer dynamics was probed by quasielastic neutron scattering and dielectric relaxation spectroscopy and was compared with that of the polymers in the bulk. In all cases, very local sub-T_g processes related to the motion of side and/or end groups as well as the segmental α-relaxation were identified with distinct differences recorded between the bulk and the confined systems. Confinement was found not to affect the very local motion in the case of the linear chains whereas it made it easier for hyperbranched polymers due to modifications of the hydrogen bond network. The segmental relaxation in confinement becomes faster than in the bulk, exhibits Arrhenius temperature dependence and is observed even below the bulk T_g due to reduced cooperativity in the confined systems.

Keywords: Polymer Dynamics, Confinement, Intercalation, Dielectric Spectroscopy, Quasielastic Neutron Scattering

---

∗ Corresponding author. E-mail: spiros@iesl.forth.gr

2

I. Introduction

The investigation of polymer dynamics has been an important and, at the same time, intriguing scientific problem over the years because of the complexity it exhibits over multiple length- and time-scales[1,2,3,4,5,6,7,8,9,10,11,12] and because of its influence on the structure-property relationship. Polymer dynamics, covers a very broad temporal range of more than 10 decades from the pico-second (ps) to the second (s) regime, whereas each type of dynamics may exhibit a different length-scale dependence that needs to be investigated.[13] A number of experimental techniques, like, e.g., neutron and light scattering, dielectric relaxation spectroscopy and nuclear magnetic resonance, have been utilized for the investigation of its temporal and/or spatial dependence.

Polymer dynamics includes vibrational motions, rotations of side groups, like hydroxyl, methyl and carbonyl groups, or other very local processes, the segmental α-process as well as the overall chain dynamics. One of the simplest types of local motion is the methyl group, $-CH_3$, rotation, which can be identified at low temperatures below the polymer glass transition, T_g.[14] At these temperatures the backbone dynamics is completely frozen and only small side groups may move. The methyl group dynamics has been investigated for several polymers, like polyisoprene,[15,16,17] poly(methyl methacrylate),[18,19] poly(isobutylene),[20,21] poly(methyl phenyl siloxane),[22,23] etc. Quasielastic neutron scattering, QENS, has been utilized to provide detailed information on the frequency of the rotation as well as on the geometry of the motion through the elastic incoherent structure factor, $EISF=I_{el}/(I_{el}+I_{quasi})$,[24] which provides a measure of the time-averaged spatial distribution of the protons; I_{el} and I_{quasi} are the integrated elastic and quasi-elastic scattering intensities, respectively. Moreover, other motions, like the hydroxyl group motion,[25,26] and the reorientation of ester groups,[27] have been probed below the polymer T_g mainly by dielectric spectroscopy; these processes follow Arrhenius temperature dependencies, $\tau = \tau_0 \exp[E/RT]$, with an activation energy E (R is the gas constant). The phenyl group dynamics has attracted the scientific interest as well, either when it is part of the main polymer chain[28,29] or when it is attached to the backbone as a pendant group;[22,30] it has been shown that the phenyl group motion consists of oscillations, π-flips and torsional processes with a broad distribution of reorientation angles.

Above the polymer glass transition temperature, the macromolecules display the segmental dynamics or alpha (α-) relaxation process, due to the cooperative motion of chain segments. Characteristic features of this process are the non-exponentiality of the respective relaxation function, expressed via the Kolhrausch-William-Watts (KWW) function $\Phi(t) =$

exp[- $(t / \tau)^{\beta}$], and the non-Arrhenius temperature dependence of its relaxation rate when approaching T_g, which is empirically described by the Vogel-Fulcher-Tammann equation, $\tau = \tau_0 \exp[B / (T-T_0)]$.[8,9,10,11,12]

The investigation of polymer dynamics close to interfaces and/or in very thin films has been a subject of great interest during the recent years, together with their static behavior, since significant differences can emerge when the molecules are confined over distances comparable to their sizes.[31,32,33,34,35,36,37,38] The equivalence in the behavior between polymer nanocomposites and thin polymer films has been quantitatively illustrated for silica / polystyrene nanocomposites.[39] Polymer nanocomposites of different dimensionalities have, thus, been utilized to investigate the effect of confinement on polymer dynamics and the resultant modifications of the polymer T_g.[22,40,41,42,43,44,45,46,47,48,49,50,51,52,53,54,55,56,57]

An intriguing class of polymer nanocomposites is the one containing layered silicates because they exhibit unique properties such as enhanced strength and thermal resistance, reduced gas permeability, reduced flammability, etc., which render them candidates for a range of applications; in these hybrids three different structures can be identified:[58,59,60,61,62] the phase separated, where the polymer and the inorganic are mutually immiscible, the intercalated, where the polymer chains intercalate between the layers of the inorganic material in an expanded multilayer structure, and the exfoliated one, where the inorganic platelets have lost their registry and are dispersed within the polymeric matrix. The structure is controlled by the interactions between the polymer and the surface of the inorganic material; understanding of these interactions allows control of the miscibility[63,64,65] and, thus, of the final properties of the nanohybrids. The interlayer galleries of the layered silicate particles are usually hydrophilic and their interactions with polar polymers are favorable. Thus, hydrophilic polymers are likely to intercalate within, e.g., sodium-activated montmorillonite clays (Na^+-MMT),[66,67,68] whereas hydrophobic polymers can lead to intercalated[69,70] or exfoliated[71] structures only with organophilized clays.

The intercalated nanocomposites, in which 0.8-2.5 nm polymer films reside between parallel inorganic layers in a well-ordered multilayer with a repeat distance of a few nanometers, constitute a very interesting class since they offer a unique avenue for the investigation of the effects of nano-confinement on polymer structure and dynamics by utilizing, however, conventional analytical techniques on macroscopic specimens. For example, a recent study on intercalated poly(ethylene oxide) / Na^+-MMT nanocomposites revealed that the polymer chains that are either confined within the galleries of the inorganic

material or are adsorbed on the outer surfaces are completely amorphous but possess significantly different conformations than those of the polymer in the melt.[72] Moreover, the kinetics of polymer crystallization is significantly altered because the surfaces induce a different nucleation mechanism.[73]

Recent studies on the dynamics of intercalated polymers reveal that the relaxation processes of the bulk polymer are strongly affected by the interaction with the inorganic layers.[22,40,43,50,74,75,76,77,78] A number of investigations showed[22,40,43,45,74,75] that the segmental relaxation process (α-relaxation) of the polymer under severe confinement appears at temperatures far below the T_g of the bulk polymer with the relaxation times being much faster than those in the bulk and exhibiting an almost Arrhenius temperature dependence. The significantly faster dynamics was discussed within the postulate of cooperatively-rearranging-regions with a characteristic length ξ; this ξ increases from small values at high temperatures to larger values as temperature decreases towards T_g with the dynamics in the bulk deviating from the Arrhenius dependence at the onset of cooperativity. Nevertheless, under confinement, this length scale cannot exceed the confining length leading, thus, to a suppression of cooperativity.[79] Alternatively, the enhanced dynamics could be attributed to an enhanced monomeric mobility[80] in an "interphase" region next to the surfaces, due to the preferential parallel orientation of the chains near the wall, with thickness that increases with supercooling. Moreover, the β-relaxation, corresponding to very local motions, was found quite similar between the bulk and the confined polymers.[22,40,43,45] In other studies, however, where the polymer-inorganic interactions are more attractive, the α-relaxation observed is much slower than that of the bulk polymer due to a thin glassy interfacial film that can be formed next to the inorganic walls.[51,76,77,78]

In this review, we will summarize some of our research work over the years on the dynamics of polymer chains severely confined within the ~1 nm interlayer galleries of intercalated polymer/layered silicate nanohybrids and the comparison with their respective relaxations in the bulk. Both hydrophilic and organophilic polymers have been utilized with the appropriate inorganic material (pristine or organophilized montmorillonite, resepctively) in order to obtain an intercalated structure. Moreover, the behavior of linear versus hyperbranched polymers has been investigated in an attempt to probe the effect of the polymer-surface interactions by altering the number and the kind of functional groups of the hyperbranched polymers. The intercalated structure of all systems was verified by X-ray diffraction whereas the dynamics was investigated by quasielastic neutron scattering and

dielectric relaxation spectroscopy. The segmental relaxation under confinement was found faster than the respective in the bulk. Moreover, it was identified even below the glass transition temperature of the neat polymers and showed an almost Arrhenius temperature dependence. More local processes, on the other hand, like relaxations of side and/or end-groups, remain unaffected by the confinement, unless the restrictions imposed to the motion by a hydrogen-bond network are altered in confinement.

II. Experimental Section

Experimental Techniques

X-ray diffraction: Structural characterization of the neat materials and the nanocomposites was performed with X-ray diffraction (XRD), using a RINT-2000 Rigaku Diffractometer. The X-rays are produced by a 12kW rotating anode generator with a Cu anode equipped with a secondary pyrolytic graphite monochromator. The CuKα radiation with wavelength $\lambda=\lambda_{CuK\alpha}$=1.54Å was used. Measurements were performed for 2θ from 1.5° to 30° with steps of 0.02°. Materials with periodic structure, like the layered silicate clays, show characteristic (*00l*) diffraction peaks, which are related to the spacing of the layers according to Bragg's law, $n\lambda=2d_{00l}\sin\theta$, where λ is the wavelength of the radiation, d_{00l} is the interlayer distance and 2θ is the diffraction angle. Intercalation of polymer chains within the silicate layers can be identified by a shift of the diffraction angle of the inorganic materials towards lower values that correspond to the increase of the interlayer distances.

Quasielastic Neutron Scattering (QENS): QENS measures the coherent, $S_{coh}(q,\omega)$, and the incoherent, $S_{inc}(q,\omega)$, structure factors as a function of the scattering vector, q, and frequency, ω. The measured incoherent and coherent scattering contributions are weighted by the corresponding neutron scattering cross sections; since the incoherent cross section of hydrogen σ_{inc}^{H}=79.9 barns is much higher than both the incoherent and the coherent cross sections, σ_{inc} and σ_{coh}, of all the other elements, the scattering is predominately incoherent[24,81] and is due to the hydrogen atoms in the specimen. $S_{inc}(q,\omega)$ is the time-Fourier transform of the intermediate incoherent scattering function $S_{inc}(q,t)$. The latter is the space-Fourier transform of the Van Hove self-correlation function $G_{self}(r,t)$ that expresses the probability that a considered particle j has experienced a displacement r during a time interval t. Herein,

6

we omit the subscripts in the notation and limit the discussion concerning the dynamics only to the incoherent contribution.

Quasielastic high-resolution neutron backscattering experiments were performed at the IN16 and IN10 spectrometers of the Institut Laue Langevin (ILL). The incident wavelength is λ=0.6271nm. The experimental resolution function, $R(q,\omega)$, is obtained by performing measurements at 2K, when the scattering of the samples within the observation window of the instrument is entirely elastic. The measured dynamic structure factor, $S_{exp}(q,\omega)$, is analyzed by assuming an elastic and a quasielastic contribution to the scattering. The latter is represented by a KWW stretched exponential relaxation function convoluted with the instrumental resolution:

$$S_{exp}(q,\omega) = A_1(q)\left(A_2(q)R(q,\omega)+[1-A_2(q)]\frac{1}{\pi}\mathcal{FT}\left\{\exp\left(-(t/\tau)^{\beta}\right)R(q,t)\right\}\right) \qquad (1)$$

$A_2(q)$ is the elastic contribution, τ is the relaxation time, whereas $R(q,t)$ was obtained analytically by fitting the instrumental resolution function $R(q,\omega)$ with a sum of a Gaussian and a Lorenzian function.[82] $\mathcal{FT}\{\ldots\}$ signifies the Fourier transform of the term in $\{\ldots\}$ and $A_1(q)$ is a multiplication factor, which accounts for the uncertainty in the exact composition of the silicates and, thus, in their scattering length density.

In addition to the quasielastic spectra, the energy resolved elastically scattered intensity from the samples is measured as a function of temperature using an identical setup of monochromator and analyzer. The elastic intensity $I_{el}(q,\omega\approx 0) = \int_{-\infty}^{+\infty} S(q,\omega)R(q,\omega)d\omega$ is recorded with the Doppler monochromator at rest corresponding to an instrumental resolution of ~1μeV. At 2K, the samples consist of essentially elastic scatterers; with increasing temperature, the molecular dynamics is enhanced, which leads to a broadening of the scattering function and a corresponding loss of the elastically scattered intensity. The scattering vector dependence of the elastically scattered intensity at each temperature can be utilized to extract the mean square displacement, $<u^2>$, according to the equation

$$I_{el}(q,\omega = 0) = I_{el}(q = 0, \omega = 0)\exp\left(-\left\langle u^2\right\rangle q^2/6\right) \qquad (2)$$

Dielectric Spectroscopy (DS): Dielectric relaxation spectroscopy measures the dielectric properties of a medium as a function of frequency.[83,84] It is based on the interaction of an external field with the molecular electric dipole moment and the determined quantity is the complex dielectric permittivity:

$$\varepsilon^{*}(\omega) = \varepsilon'(\omega) - i\varepsilon''(\omega) \tag{3}$$

where ε' represents the real part and ε'' the imaginary part or the energy loss part, $\omega = 2\pi v$ and v the measured frequencies. The measured ε^* is given by the one-sided Fourier transform of the time derivative of the dipole-dipole correlation function C(t), which probes local motions for non-zero dipole moment perpendicular to the chain contour.

The dynamic measurements were performed utilizing a Novocontrol dielectric spectrometer, in the frequency interval 10^{-2}–10^7 Hz. A film (hundreds of nanometers) of the material under study was placed in a stainless steel parallel plate capacitor. The temperature was controlled through a heated flow of nitrogen gas, by Quatro Cryosytem in the range 143–433 K. During measurements, samples were kept in a pure nitrogen atmosphere. All samples were kept at the highest starting temperatures for 30 min before the measurements began and were thermally equilibrated at successively decreasing temperatures prior to data collection.

The $\varepsilon^{*}(\omega)$ data were analyzed utilizing the empirical Havriliak-Negami (*HN*) functions:[84]

$$\varepsilon^{*}(\omega) = \varepsilon_{\infty} + \Delta\varepsilon \ / \ [1+(i\omega\tau_{HN})^{\alpha}]^{\beta} \tag{4}$$

where τ_{HN} is the characteristic relaxation time, $\Delta\varepsilon = \varepsilon_0' - \varepsilon_\infty'$ is the relaxation strength of the process and α, β ($0 < \alpha$, $\alpha\beta \leq 1$) describe the symmetric and asymmetric broadening of the distribution. An additional ionic conductivity contribution at low-frequencies and high temperatures is accounted for by an ω^{-1} dependence. Alternatively, the experimental $\varepsilon''(\omega)$ were inverted[85] based on a modification of the CONTIN program,[86] to determine the distribution of relaxation times $\tilde{F}(\ln\tau)$ assuming a superposition of Debye processes:

$$\varepsilon''(\omega) = \int \tilde{F}(\ln\tau)\left\{\omega\tau / \left[1+(\omega\tau)^{2}\right]\right\} d(\ln\tau) \tag{5}$$

where the integral of $\tilde{F}(\ln\tau)$ results in the dielectric strength $\Delta\varepsilon$ and the most probable relaxation times correspond to the maxima of $\tilde{F}(\ln\tau)$.

Alternatively, the electric modulus, $M^{*}(\omega) = 1 \ / \ \varepsilon^{*}(\omega)$, representation of the dielectric data can be used; in the latter case the ionic mobility can be extracted in addition to the polymer mobility.

III. Results and Discussion

In the following, we are going to discuss in some detail the dynamics of three different systems, an organophilic linear poly(methyl phenyl siloxane), a hydrophilic linear

poly(ethylene oxide) and a series of hyperbranched polymers, in bulk and under severe confinement within the galleries of layered silicates. The discussion will be based on our investigations on these systems but it will put these works in the context of other works in this field as well. We will examine the dynamics over multiple length and time scales such as the methyl group rotation, the rotation and/or reorientation of small side groups (usually referred as γ- and β-relaxation) as well as the segmental α-relaxation, which is due to the cooperative motion of a few segments of the chains and which is related with the glass transition. The processes which are observed in the confined systems and are found to exhibit a different behavior than the respective ones in the bulk will be noted with a prime in the corresponding letter of each relaxation process.

Organophilic linear PMPS

Poly(methyl phenyl siloxane), PMPS, is a polymer that possesses both a methyl group and a pendant phenyl ring (Scheme 1), so it shows rich dynamics both below and above the calorimetric glass transition temperature. A few studies exist in the literature where experimental techniques, like quasielastic neutron scattering,[22,30, 87] dielectric relaxation spectroscopy,[87,88] and light scattering[89,90] have been utilized; nevertheless, the majority of them were related to the dynamics of PMPS in the bulk and only few to the relaxation of PMPS under confinement.[22,40,43,44,48,91]

Figure 1 shows the X-ray diffractograms of the organophilized silicate[92] and the PMPS nanohybrids with different polymer concentrations prepared by melt mixing.[22,40,93] The amorphous PMPS (not shown) exhibits only a weak amorphous halo whereas the organosilicate shows a main diffraction peak at $2\theta=3.5\pm0.1°$, which corresponds to an interlayer distance of $d_{001}=25.0\pm1.5$Å. This peak is relatively broad and the first and second maxima are not exactly equidistant in the 2θ scale, which indicates that the coherence of the organoclay structure is not high.[94,95] Additionally, discontinuities and/or defects located at the boundaries of the silicate tactoids were found responsible for the not-perfect diffraction pattern.[95] The shift of the main peak to an angle $2\theta=2.45\pm0.1°$ for the nanocomposites is due to the intercalation of the polymer chains within the galleries of the inorganic material. The nanocomposite spacing is $d_{001}=36.0\pm1.5$Å, i.e., it has increased by ~10Å for all hybrids independently of the polymer content. For all these nanocomposites but the one with 70wt% PMPS, it is estimated that the polymer chains are mostly intercalated within the galleries without much polymer residing outside the completely filled galleries.

The dynamics of the confined polymers in hybrids with low polymer content were investigated early on utilizing dielectric relaxation spectroscopy[40] and compared to that in the bulk. Since PMPS possesses a dipole moment perpendicular to the main chain, its segmental motion is dielectrically active. The dielectric loss data for bulk PMPS showed a single relaxation process above 223K, i.e., above the polymer glass transition temperature,[40] which exhibited a strong temperature dependence and could not be measured above 258K because it became too fast. On the other hand, the dielectric spectra of the nanohybrids showed the presence of dynamics even at temperatures much below the bulk polymer T_g; the process exhibited a very weak temperature dependence and was observed within the accessible frequency window for temperatures 173-243K. The shape of the relaxation process was quite similar with the process observed in bulk PMPS with only a weak dependence on temperature observed in the hybrids in contrast to its insensitivity in the case of the bulk polymer. It is noted that the dielectric loss for the silicate was very broad and its contribution was subtracted from the spectra of the nanohybrids before the analysis.

Figure 2, shows the most probable relaxation times, obtained from the analysis of the experimental dielectric loss data according to Eq. 5, in an Arrhenius representation for both the bulk and the confined PMPS.[40] The solid line represents the relaxation times of the bulk PMPS that corresponds to the segmental α-relaxation observed above T_g; the temperature dependence follows the Vogel-Fulcher-Tammann (VFT) equation $\tau = \tau_0 \exp[B / (T-T_0)]$, with $\tau_0 = 1.7 \times 10^{-13}$s the microscopic time, B=440±30K the activation energy parameter and T_0=195±2K the Vogel temperature. The dynamics of confined PMPS was, however, intruiging.[40] A very fast process was found to dominate the dielectric spectra. This process showed a very weak, almost Arrhenius, temperature dependence; its dynamics appeared to merge with the dynamics of the bulk PMPS at high temperatures whereas it was almost six orders of magnitude faster than the bulk segmental process in the proximity of the bulk T_g. Moreover, it was observed for a broad range of temperatures even below the bulk T_g. The attempt to analyse the relaxation times of this process with a VFT equation resulted in a Vogel temperature of T_0=93±2K, i.e., ~100K lower than in the bulk, and an activation energy parameter of B=962±20K more than double than the one of the bulk; the microscopic time is $\tau_0 = O(10^{-13}$s). The fragility parameter, $D=B/T_0$ is 2.3 for PMPS whereas it becomes D=10.3 for the confined chains indicating that the confined PMPS behaves as a stronger glass (more Arrhenius-like), i.e., confinement influences a conformational rearrangement. This relaxation process observed in all PMPS hybrids is considered as the modified segmental relaxation of

the confined PMPS and is noted as α'-process from here on. At high temperatures, a slow process was evident with a weak dielectric strength and its relaxation times coinciding with the ones of the bulk polymer; most probably, this was due to the segmental motion of PMPS, which lied outside the galleries of the nanocomposites. Finally, an intermediate process appeared in the same frequency range with a process observed in the bare inorganic material, which remained either due an imperfect subtraction or due to an enhanced dielectric strength in the nanohybrids.

The fast dynamics can be understood within the postulate of cooperatively rearranging regions with a characteristic length-scale ξ,[79] which is temperature dependent. According to this model, at high temperatures, ξ is small and, thus, no difference should be expected between bulk and confined PMPS. As temperature decreases towards T_g, the dynamics deviate from the Arrhenius temperature dependence at the onset of cooperativity. In the bulk, ξ increases unhindered as $\xi = \xi_0 [T / (T - T_0)]^{2/3}$, whereas, in the confined systems, the increase is limited by the confining length $d \sim 1$nm (in the current case). Actually, an attempt for the quantitative verification of such an assumption was performed;[79] the bulk PMPS data were analyzed within the coupling model and the primitive relaxation times τ_0 were estimated. For temperatures above T_g, the values of τ_0 and of the relaxation times of the confined polymer coincided illustrating the lack of cooperativity for the confined system. Alternatively, the existence of faster dynamics could be discussed in terms of the chains adopting a parallel configuration next to a wall with oscillations in the monomer density profile causing a dynamic anisotropy with enhanced parallel and reduced perpendicular monomeric mobilities extending over distances, which increase with supercooling. Under severe confinement, this "interphase" extends over the whole film, thus, leading to fast dynamics.

Dielectric relaxation spectroscopy is a macroscopic technique; thus, quasielastic neutron scattering, a technique that can probe dynamics over different length scales (correlated with its range of scattering wavevectors), was employed to extent the investigation of the dynamics of PMPS under confinement. PMPS possesses both a methyl group and a pendant phenyl ring; thus, its dynamics corresponds to the methyl group rotation, the phenyl group flips as well as the segmental relaxation. The study of the nanohybrids probes the influence of confinement on all these different processes.

Energy-resolved elastic scattering and dynamic quasielastic measurements were performed over a very broad temperature range.[22] Figures 3a-c show elastic temperature scans for PMPS, for the organosilicate and for a PMPS nanohybrid with 25wt% polymer

content (PMPS25) at various wavevectors. All curves are normalized to the data at the lowest temperature. For the bulk polymer, two distinct relaxation steps, especially pronounced at high wavevectors, were evident in the energy-resolved elastically scattered intensity. The first step at temperatures between 50-150K was attributed to the rotation of the methyl side groups attached to the polymer chains whereas the second one at temperatures higher than the calorimetric T_g of the polymer was assigned to polymer segmental motions, which become unfrozen near and above the polymer T_g. The data for the silicate exhibited a continuous decrease with increasing temperature. This decrease could be attributed to the motion of the protons of the surfactant chains used for rendering the surface of the silicate organophilic, which gradually became unfrozen at temperatures above ~150K. The temperature dependence of the elastic scattering intensity for the PMPS25 nanocomposite exhibited two relaxation steps as well, similar to the ones observed for the bulk PMPS: a step at the temperature range (50-150K) of the methyl group rotation and a very broad decrease at temperatures in the range of the bulk polymer T_g. If one attempted to compose a weighted average of the contributions from the silicate and the bulk PMPS, a close agreement was achieved only in the range of the methyl rotation but not at higher temperatures. The step in the composed weighed scan is much narrower near T_g in comparison to the measured scan for the composite, indicating the onset of mobility for the confined polymer at temperatures lower than in the bulk.[22]

The wavevector dependence of the elastic intensity at each temperature provides the mean square displacement, $<u^2>$, according to Eq. 2. Figure 3d shows $<u^2>$ for the PMPS, the organosilicate and the nanocomposite PMPS25 as a function of temperature. The temperature dependence of the mean square displacement clearly illustrates the discussion above on the elastically scattered intensity. For bulk PMPS, $<u^2>$ first increased with temperature above ~50K, as the methyl group motion becomes active, it reached a plateau when this motion became too fast for the time window of the IN16 spectrometer, it subsequently increased again when the second kind of motion became active and, finally, it appeared to approach a second plateau like region at high temperatures. The $<u^2>$ of the organosilicate was almost zero up to about 150K whereas it began to increase gradually above this temperature due to the gradually increasing mobility of the surfactant chains. The data of the nanocomposite superimposed perfectly with the data for the homopolymer in the temperature range where the methyl rotation was observed, which was apparently exactly the same for both bulk and confined PMPS. In contrast, the behavior of $<u^2>$ near the T_g exhibited differences between

12

the nanocomposite and the bulk homopolymer. For the nanocomposite, the second increase began at temperatures below the T_g of the pure polymer and $<u^2>$ attained values much higher than the respective ones for bulk PMPS. This, in principle, agrees with enhanced mobility and an apparently lower effective glass transition temperature for the confined system; however, differential scanning calorimetry (DSC) measurements do not trace any thermal transition for PMPS25. Nevertheless, since the enhanced mobility could be related to the observed mobility of the surfactants in the organosilicate near T=150K, the sum of $<u^2>$ of the pure polymer and the silicate was calculated and compared with the $<u^2>$ of PMPS25. This sum, represented as the solid line in Fig. 3d, more or less followed the data for the $<u^2>$ of PMPS25 in the low temperature regime but above ~220K (close to the bulk polymer T_g) the $<u^2>$ of the nanocomposite deviated significantly from it, indicating accelerated dynamics.

Quasielastic neutron scattering measurements were performed at temperatures that cover both regimes to probe the methyl rotation and the segmental motion.[22] Figure 4a shows the incoherent structure factor of PMPS and PMPS25 at T=100K, well below the bulk T_g, for a wavevector q=1.1Å^{-1}. The two measurements are very similar, especially in the quasielastic wings, and differ only in the elastic scattering intensity. The instrumental resolution measured at T=2K, where all scatterers are frozen, is included to illustrate that there is a small but considerable broadening and, thus, dynamics in both PMPS and PMPS25. The spectrum of the organosilicate at this temperature, on the other hand, coincided with the resolution (times a multiplication factor), which means that there is no molecular dynamics within the present frequency window; thus, whatever motion is probed in the nanocomposites is related to the moving protons of the confined polymer. The motion that corresponds to the spectral broadening in this temperature range should be associated with a local motion, the methyl group rotation.[22] Fitting the experimental data with Eq. 1 (Fig. 4a) provides the elastic and the quasielastic contributions to the spectra as well as the relaxation time of the motion. The wavevector dependence of the average relaxation times for PMPS and PMPS25 for different temperatures below T_g are shown in Figure 4b. The average relaxation times, τ_{ave}, are calculated using the estimated characteristic times of the KWW function of Eq. 1, $\tau = \tau_{KWW}$, as

$\tau_{ave} = \int_0^\infty \exp\left[-\left(t/\tau_{KWW}\right)^\beta\right]dt = \left(\tau_{KWW}/\beta\right)\Gamma(1/\beta)$, where β is the stretching exponent and

$\Gamma(x)$ the Gamma function with argument x. It is clear that, over the wavevector range covered by IN16, the relaxation times are independent of the wavevector q, verifying that it is a very local process. The relaxation times become faster with increasing temperature with the data exhibiting an Arrhenius temperature dependence with the activation energy E_{methyl} =

2.90±0.30 kJ/mol, which is somehow smaller than the values quoted for methyl rotation in other systems.[15,16,17] The relaxation times obtained for PMPS25 at T=100K were only slightly faster than the respective ones of the bulk polymer (Fig 4b), in agreement with the elastic measurements indicating that such local processes are not affected by the confinement.

The situation changes as the temperature increases in the range of the bulk polymer T_g where other motions become active. For the polymer in the bulk, the data illustrated the absence of any dynamics within the frequency window of IN16 for temperatures between 120K and 220K, whereas the dynamics at 240K was attributed to the phenyl ring flips and that at 300K was assigned to a clear α-relaxation; between 240 and 300K, a coupled phenyl flip and segmental motion contribute to the spectra. At T=300K, the relaxation times decrease with increasing wavevector as $\tau_{ave} \sim q^{-2.60\pm0.40}$, in contrast to the q-independent relaxation times of the methyl group rotation but in agreement with the expected behavior of the segmental relaxation; the relaxation times for the segmental relaxation at 300K are in a relatively good agreement with those of earlier studies on PMPS.[30,88,96] A clear difference is observed in the dynamic behavior of the nanohybrid. Whereas, at T=220K the dynamics of bulk PMPS were too fast to be measured, the data for the PMPS25 nanocomposite exhibit a broadening due to some kind of molecular dynamics in agreement with the mean-squared displacement data in Fig. 3d, which showed that $<u^2>$ for PMPS25 deviated from the plateau of the PMPS and already began to increase at temperatures ~175-180K. Nevertheless, a broadening of the incoherent structure factor was also observed for the silicate at 220K, which, when analyzed, resulted in a quasielastic contribution that was very similar to the respective one for the nanocomposite. It was, thus, apparent that the observed dynamics in the nanocomposite at this temperature was significantly influenced by the motion of the surfactant chains utilized to render the silicate surfaces organophilic. The behavior was quite similar at even higher temperatures and one, thus, had to conclude that the observed process in the nanocomposites was a coupled motion between the motion of the confined polymer and that of the surfactant chains, which contain an abundance of hydrogen atoms.

Thus, it is assumed that the very local methyl group rotation is not affected by the confinement whereas above T_g, the effect of spatial restriction cannot be investigated in this system. The former conclusion, i.e. the fact that the local motion does not depend on the confinement was demonstrated, as well, by comparing the mean squared displacement of PMPS homopolymers of different molecular weights in the bulk and under confinement either between the platelets of layered silicates or within porous glasses of different pore size

in the range between 2.5-7.5 nm.[43] For temperatures up to T=150K, there was a very good superposition of all mean squared displacement values, $<u^2>$; moreover values for $<u^2>$ of poly(dimethyl siloxane), PDMS, in the bulk and confined in porous glasses were superimposed as well with the ones of PMPS when the number of slower protons of the phenyl group (in the PMPS) was taken into account. For temperatures above the glass transition temperatures of the polymers, deviations in the superposition of the $<u^2>$ of the various systems were observed. The dynamics of PMPS confined in porous glasses was investigated in detail as well by dielectric spectroscopy and quasielastic neutron scattering and the results were compared to the ones in the bulk.[44,48,91] For pores up to 7.5 nm, the relaxation rates were found to follow a VFT temperature dependence whereas for a pore size of 5 nm this dependence became Arrhenius with a low activation energy. The relaxation times are faster for low temperatures and cross the ones of the bulk at higher temperatures. Moreover, thermally stimulated differential scanning calorimetry[48,91] showed that at the same pore size, ΔC_P vanishes, indicating a dramatic change in the character of the motion and supporting the existence of a characteristic length scale for the cooperativity of the motion to set in. These results were in agreement with QENS findings on the mean squared displacement, which decreased with the confinement. Similar investigations were performed for PDMS and poly(propylene glycol) with basically similar results. In the latter case,[97,98] the critical length-scale for cooperativity was smaller than that of PMPS with values ~1.6-1.8nm, whereas an interplay between confining and adsorption effects was observed depending on the pore size.

In order to overcome the complications due to the surfactant molecules and to be able to study the segmental dynamics of the polymer under severe confinement in the absence of any coupling, nanocomposite systems without surfactants should, in principle, be utilized. Such a case is that of a hydrophilic polymer that can intercalate within the layers of hydrophilic silicates. Along these lines, the dynamics of poly(ethylene oxide) homopolymer severely confined between the layers of sodium-activated montmorilonite, Na$^+$-MMT, was investigated.

Hydrophilic linear PEO

Poly(ethylene oxide), PEO (Scheme 2), is a nonionic, water soluble, semi-crystalline polymer with many applications due to its flocculent, thickening, sustained-release,

lubrication, dispersing, and water-retention properties. Its hydrophilicity, biocompatibility and versatility make it attractive as a biomaterial as well. Additionally, PEO is a favorable candidate for the development of solid polymer electrolytes with high ionic conductivity because of its ability to dissolve large amounts of salt and because of its structure, which supports ion transport.[99,100,101,102,103] Despite its pronounced crystalline character that hinders cation mobility, PEO-based electrolytes are still among the most studied polymer ionic conductors, with various methods having been developed to increase the fraction of its amorphous phase and improve its conductivity at ambient temperatures.[101,104] A promising way to control polymer crystallinity is the incorporation of inorganic nanoparticles such as nanoclays;[72,100,105,106] this can additionally increase the mechanical and thermal stability of the material and, thus, improve its final performance. Investigation of PEO intercalated within lithium-activated montmorillonite, Li^+-MMT, by solid state ^{2}H-NMR[100] and thermally stimulated depolarization current[66] revealed that both the local and the global dynamics of PEO confined between the layers of layered silicates are dramatically different from those in the bulk.[101,102,107] On a local scale, intercalated polymer chains exhibit higher flexibility along their backbone with a marked suppression (or even absence) of cooperative dynamics typically associated with the glass transition. On a global scale, relaxation of polymer chains either tethered to or in close proximity (<1 nm as in intercalated hybrids) to the host surface are dramatically altered and parallel those of other intrinsically anisotropic materials such as block copolymers and liquid crystals. ^{2}H NMR measurements of perdeuterated PEO in the bulk and when intercalated in 0.8nm gap between the layers of Li-fluorohectorite showed that motion starts to develop at lower temperatures indicating increased segmental motion for the confined polymer. Nevertheless, despite the behavior at low temperatures, at higher temperatures the layered silicates seem to restrict motion so that some local configurations of the chains are not accessible.[102,107] Moreover, differential scanning calorimetry and thermally stimulated current measurements show no clear peak in the spectra of the intercalated PEO in the temperature range of the bulk glass transition temperatures indicating that cooperative relaxations, even if present, are very weak.[66,107] Additionally, the dynamics of PEO has been studied when the chains are confined within laponite,[76] the pores of anodic aluminium oxide,[108] graphite oxide,[53,54,109] or between the layers of other polymers[110] with sometimes contradictory results.

        The PEO segmental motion was probed in a PEO/laponite intercalated phase, over the tens of microseconds time scale, using ^{13}C and ^{1}H solid state NMR.[76] A significant slowing down of the motion was observed, as compared to the local dynamics in the amorphous phase

of bulk PEO whereas strong dynamical heterogeneities in the intercalated PEO are still observed even at room temperature. This decrease in the segmental mobility was attributed to the complexation of PEO oxygens by the Na^+ counterions in the laponite galleries, which act as physical crosslinks. In another investigation, the structure and dynamics of end-labeled PEO intercalated within the galleries of a fluoromica inorganic clay were studied by spin-label electron spin resonance (ESR).[111] For low PEO content and confining length of 0.33nm, the ESR spectra indicated a very low segmental mobility even at high temperatures, which was attributed to the strong polymer interactions with the charged mica surfaces. For higher polymer content and confining length of 0.83nm, both a slow and a fast motional component were observed attributed to segments located close to and away from the solid walls within the galleries. Moreover, the activation energy of the fast segmental motion was lower than that of the bulk PEO. This fast motion with the low activation was attributed to a reduced segmental density and reduced cooperativity of the confined PEO chains. Confinement of PEO was investigated when the PEO chains have been intercalated between the layers of graphite oxide, GO, as well.[53] In that work, it was shown that the intercalation of polymer chains does not only lead to the suppression of polymer crystallization but also in the suppression of the dielectric α-relaxation that is related to the glass transition together with a slowing down of the β-relaxation modes. The fact that no segmental relaxation could be observed suggests the lack of cooperativity among intercalated PEO chains in agreement with the results described above. In order to identify the two processes, the dynamics of short PEO chains of different molecular weights were investigated in the bulk and under confinement within the GO galleries utilizing dielectric spectroscopy.[54,109] In the bulk, two molecular weight dependent processes were obtained, identified at the β- and α-relaxation. Two processes are found under confinement as well; however, they are observed at different time scales and with different dependencies. The relaxation times of the fast process under confinement do not show any dependence on the chain length but they exhibit a change in the activation energy of the Arrhenius temperature dependence. At higher temperatures, the obtained activation energy resembles the one of the bulk whereas, at lower temperatures, a lower activation energy is obtained attributed to a different conformation of the chains within the galleries. The slow motion is much slower that the bulk segmental relaxation and it is attributed to interfacial polarization. The authors correlated the absence of the segmental relaxation under confinement with the absence of any detectable glass transition in these systems indicating lack of cooperativity.

At the same time, molecular dynamics computer simulations revealed that PEO adopts highly amorphous conformations in a liquidlike bilayer inside the galleries of montmorillonite and shows no indication of crystallinity or periodic ordering; confined chains are less ordered than the most disordered bulk PEO system due to both the severe confinement and the coordination of the ether oxygens with the alkali cations in the galleries.[67,112] Moreover, a coexistence of fast and slow relaxation times was observed for the nanoscopically confined chains, over a wide temperature range, in agreement with NMR measurements. This was attributed to fast relaxing C–H segments, primarily present in regions of low local density and no/few coordinated lithiums, whereas lithium coordination to the ethylene oxide groups resulted in anchoring chains on the confining walls, inducing solidlike segmental dynamics even at high temperatures.[113]

The dynamics of a series of PEO/Na^+-MMT nanocomposites with polymer content that covered the whole range from pure polymer to pure clay, prepared utilizing melt intercalation, has been investigated as well.[45,72,114,115] Figure 5 shows the XRD measurements of the pure PEO, the Na^+-MMT and the nanohybrids.[45,72] Pure Na^+-MMT exhibits a main (001) diffraction peak at $2\theta=8.8°$, which corresponds to an interlayer distance of ~1.0 nm. Upon addition of PEO, the peak shifts towards lower angles due to the polymer intercalating within the inorganic galleries. For PEO/Na^+-MMT with polymer content 30wt% and higher, the diffraction peak has shifted to $2\theta = 4.8°$ corresponding to an interlayer distance of ~1.85 nm. In this concentration range, bi-layers of intercalated PEO chains exist within the galleries, in agreement with computer simulations.[67] For lower PEO content, mono-layers of polymer chains were also observed inside the galleries with an interlayer distance of ~1.3nm. In all cases, the presence of diffraction peaks that correspond to higher order reflections evidences the coherence of the intercalated structure.[72]

Poly(ethylene oxide) is a semi-crystalline polymer that crystallizes in a monoclinic unit cell. Its crystalline structure has been studied in the past with a series of experimental techniques like XRD and infrared and Raman spectroscopies. The X-ray data for bulk PEO (Figure 5) show a series of crystalline diffraction peaks with the scattering angles of the main ones observed at $2\theta=19.0°$ and $2\theta=23.1°$ in a very good agreement with those reported in the literature. [116, 117, 118, 119] The diffractograms of the nanocomposites showed peaks that correspond to crystalline PEO only for polymer concentrations higher than ~70 wt%. The absence of these diffraction peaks from the data of the nanocomposites with lower PEO content indicates that the intercalated polymer as well as the chains that are in close proximity to the inorganic surfaces are amorphous; it is only the excess polymer outside the

completely filled galleries and away from the outside walls of the inorganic particles that is able to crystallize. Thus, the crystallinity drops abruptly to zero at a specific composition of the nanohybrids; this is verified by DSC as well as infrared and Raman spectroscopies.[72] The existence of a disordered liquid-like structure inside the galleries has been predicted by computer simulations as well.[67] Furthermore, it was found that the conformation of the confined chains are significantly modified from the bulk polymer in the melt and that the number of gauche conformations and, thus, the disorder of the structure increases in confinement.[72] Note that a similar series of nanocomposites prepared utilizing solution intercalation gave exactly the same results, thus, certifying the attainment of equilibrium in both cases.

The polymer dynamics in the intercalated hybrids was investigated utilizing dielectric relaxation spectroscopy in the frequency range 10^{-2} to 10^6 Hz.[45] Figure 6 shows the imaginary part of the electric modulus, $M''(\omega)$, as a function of frequency for pure PEO and different PEO/Na$^+$-MMT nanohybrids at 203 K, i.e., close to the bulk polymer T_g.[45] At this temperature, a local β-process and a segmental α-process are evident in the spectrum of the bulk PEO. A process appears, however, in the nanocomposites at intermediate frequencies, which is termed α'; this process gains intensity in the composites at the expense of the slower α-process. Moreover, although the β-process is present at all nanocomposite spectra, the α-process is observed only in the polymer-rich composites, i.e., in nanohybrids with both intercalated and excess PEO chains outside the galleries. This behavior is very similar to the one observed in the dielectric measurements of confined PMPS, discussed above.

The most probable relaxation times of the PEO/Na$^+$-MMT hybrids are shown in Figure 7 as exemplary cases of the rich nanocomposite dynamics.[45] The relaxation times of the α-process for bulk PEO conform to the Vogel-Fulcher-Tammann equation $\tau = \tau_0 \exp[A / (T-T_0)]$, with $\tau_0 = 1.0 \times 10^{-11}$s the high temperature intercept, B=2700 K the activation energy parameter and $T_0 = 112 \pm 10$K the Vogel temperature. The relaxation times for the β-process of the pure PEO follow an Arrhenius temperature dependence with a single activation energy E=35 kJ/mol. For the PEO/Na$^+$-MMT 50/50 hybrid as well as for all hybrids with lower PEO content, the usual PEO α-process is not observed at all. The PEO segments are all confined within the galleries and relax with the faster α'-process, which exhibits an Arrhenius temperature dependence with a single activation energy.[45] The fast local β-process is observed with a rate comparable to that of bulk PEO due to its local character. In contrast, for the PEO/Na$^+$-MMT 70/30 and 80/20 composites, with excess PEO outside the galleries, both

the α- and β-processes are observed almost identical to those of pure PEO. This α-process is due to the segmental motion of the amorphous regions of the PEO chains that reside outside the galleries and crystallize similarly to bulk PEO. The α'-process, with dynamics intermediate between the α- and β-processes, is observed in these systems as well, with dielectric strength that is an increasing function of the clay content, i.e., of the ratio of confined to unconfined chains. The process is due to PEO confined within the galleries. The activation energies of the Arrhenius α'-process vary systematically from 28±3 kJ/mol for the 80/20 to 12±2 kJ/mol for the 30/70.[45]

The main finding, i.e., the existence of a relaxation process intermediate between the α- and β-processes, which exhibits Arrhenius temperature dependence and is due to the segmental motion of the confined chains, is in a very good agreement to what was observed in the case of the organophilic PMPS.[40] Nevertheless, the α'-process in PEO/Na$^+$-MMT follows an Arrhenius dependence which should be contrasted with the weak VFT one observed in confined PMPS. This may reflect the fact that bulk PEO is less fragile than PMPS with a steepness index m ($=d[\log\tau(T_g)]/d(T_g/T)$ at $\tau(T=T_g)\cong1$ s) of 22 compared to 73 for PMPS.[40] Alternatively, it may be due to the different inter-molecular cooperativities of PEO and PMPS: PEO, with the small monomeric volume and flexible backbone, is expected to be predominantly intra-molecularly cooperative[120] whereas PMPS, bearing a bulky side chain, more inter-molecularly cooperative.[121,122] Thus, $\xi_{PEO}<\xi_{PMPS}$, giving rise to the observed Arrhenius dependence. At the same time, the relaxation times of the confined systems are found to be in a very good agreement with the primitive relaxation times of bulk PEO, calculated based on the coupling mode, thus indicating a lack of cooperativity.[123] Moreover, the local β-process is not affected by the confinement, similarly to the local methyl group rotation (a motion that is not dielectrically active) probed by QENS for PMPS.

Quasielastic neutron scattering measurements were performed in these systems as well to investigate the dynamics of bulk and confined PEO. [124, 125] Figure 8a shows temperature scans of the energy resolved elastic intensity measured on IN16 for the PEO homopolymer, the Na$^+$-MMT silicate, and the nanocomposite with 30wt% PEO at $q=1.29\text{Å}^{-1}$. The energy-resolved elastic intensities were normalized to the value at T=2K where all dynamics is frozen. The scan for PEO exhibits two distinct relaxation steps. The first starts above T=200K and is related to the segmental motion of the amorphous portion of the semi-crystalline homopolymer above its T_g. The second is an abrupt drop of the intensity at the PEO melting temperature, T_m, which indicates that the polymer motion has become much

20

faster than the energy resolution. The data for the silicate exhibit a continuous small decrease with increasing temperature around the T_m of water and almost reach a plateau at high temperatures. The intensity for the nanocomposite exhibits a broad decrease, whereas there is no evidence of a sharp drop due to melting similar to the one observed for the homopolymer, in agreement with XRD and DSC results that indicate that at the specific composition there is no crystalline PEO present in the specimens.

Quasielastic measurements were performed for temperatures between T_g and T_m for the bulk PEO and even above the bulk T_m for the nanohybrid, following the findings of the elastic measurements. Figure 8b shows quasielastic spectra of the three samples at T=345K, which is above the melting temperature of bulk PEO.[124,125] The figure shows the inelastic wings (10% of the maximum intensity for the silicate) of the spectra whereas the instrumental resolution is included for comparison. For the homopolymer, very weak scattering is observed resembling a weak constant background indicating that all motions of the PEO are too fast (faster than 50ps) to be reliably determined by IN16. The data for the silicate cannot be distinguished from the resolution indicating no dynamics within the accessible dynamic range. The presence of dynamics within the experimental window is clear for the confined system. Analysis of the QENS data for the nanocomposite with Eq. 1 results in a process with relaxation time τ_{ave}=193ps for the intercalated polymer that has been strongly affected by the confinement. It is noted that, at temperatures well below the T_m of bulk PEO, the dynamics of the bulk and the confined polymer was very similar. Since for temperatures above the PEO melting temperature, the polymer dynamics were too fast to be determined by IN16, measurements were performed at spectrometer IN6, which has different resolution.[125] This provided the opportunity to combine measurements from two different spectrometers and, thus, increase the accessible time range over which one can probe the dynamics.

Quasielastic neutron scattering was also utilized to investigate the dynamics of a linear hydrophilic glassy polymer, poly(hexa(ethylene glycol) methacrylate)), PHEGMA, intercalated within Na$^+$-MMT.[75] Both elastic and quasielastic measurements were performed and showed that the confined system exhibited much weaker temperature and wavevector dependencies of the elastic intensity and of the respective relaxation times. The mean square displacement in confinement in the neighborhood of the glass transition begins to increase at temperatures well below the bulk polymer T_g, indicating enhanced mobility when compared to the bulk polymer.

Therefore, in the case of linear polymers weakly interacting with the silicate surfaces, confinement leads to faster segmental dynamics with weak temperature dependencies,

whereas the very local motions remain practically unaffected. Next, the effects of confinement on the dynamics for more complex polymer architectures, like hyperbranched polymers, were investigated in order to probe the effects of both the architecture and of the varying interactions with the inorganic surfaces via the functional groups existing in the molecules peripheries.

Hyperbranched Polymers

Hyperbranched polymers, HBPs, are a relatively new category of highly branched materials, which have three dimensional tree-like structure and polydispersity.[126,127,128,129] HBPs show unique features, like low viscosity at high molecular weight, high solubility, miscibility and reactivity influenced by their end groups, whereas they have the additional advantage of a cost-effective synthesis when compared to dendrimers due to their one-pot synthetic method and the lack of need for tedious purification procedures. HBPs can be used in industrial applications,[130] as additives in coatings,[131] membranes[132] and batteries,[133] as nanoscale catalysts, as additives in conventional epoxy resins,[134] as well as in the pharmaceutical industry and medicine for the encapsulation of substances, targeted delivery of drugs, as therapeutic agents, as *in vitro* diagnostics for cardiac testing, contrast agents for MRI, etc.[135,136] Up to now, their dynamics have been investigated experimentally in the bulk mainly for temperatures lower that the glass transition temperature[137,138,139,140] utilizing dielectric spectroscopy. Moreover, atomistic molecular dynamics simulations were performed to examine the static and dynamic properties of HBPs in the melt over many length- and time-scales and to investigate the formation and lifetime of intra- and inter-molecular hydrogen bonds.[141,142] Only recently their dynamics under confinement has attracted the scientific interest showing both similarities and differences with that in the bulk as well as a significant influence of the hydrogen bonds on the dynamics to be discussed herein.[54,57]

Figure 9 shows the XRD data of hybrids composed of Na^+-MMT[115] and the hyperbranched polyesteramide Hybrane[55,143,144,145] (Scheme 3[144]) as well as three generations (H20, H30 and H40) of the hyperbranched polyester polyol Boltorn[57,146] (Scheme 4) together with the diffractogram of the pure clay. All samples have been prepared by solution mixing and slow solvent evaporation following by thermal annealing for 24h at 200°C in a vacuum oven to erase any metastable structures formed during solvent evaporation and achieve equilibrium. Hybrane is amorphous and its diffraction pattern (not shown[55]) exhibits only a weak amorphous halo. The three Boltorns (not shown[57]) exhibit a weak peak superimposed

on the broad amorphous halo that corresponds to a distance of ~0.5 nm indicating a chain packing of the polymers probably due to a strong hydrogen bond network.[136,147,148] The XRD patterns of all the nanohybrids clearly indicate intercalated structures in all cases since the diffraction peak of Na^+-MMT that corresponds to a 1.0±0.05nm d-spacing shifts towards lower angles in the hybrids; the 30 wt% Hybrane nanohybrid shows an interlayer distance of 2.10±0.05nm whereas the 50wt% Boltorn/Na^+-MMT nanocomposites show d-spacings of 1.95±0.05 nm for H20, 2.05±0.05 nm for H30 and 2.15±0.05 nm for H40. Thus, a confined polymer film of ~1nm thickness is present for all hybrids consisting of polymer bi-layers,[55,57] whereas it can be safely estimated that there is no significant excess of polymer outside the completely filled galleries These systems are, thus, selected for the investigation of the dynamics of hyperbranched polymers in confinement.

The dynamics of Hybrane and the hybrid with 30wt% polymer were investigated with quasielastic neutron scattering.[55] The energy resolved elastic scattering for the polymer in the bulk shows first a broad decrease at temperatures between ~80 and 220K and a second step at temperatures higher than the calorimetric T_g.[55] At the low temperatures, the main chain is still frozen, so the intensity drop is due to local sub-T_g dynamic processes, which can be attributed to the more mobile end- and/or side-groups, i.e., the methyl and the hydroxyl groups attached to the polymer backbone. It is noted that the intensity drop herein is observed over a broader temperature range than that corresponding to simple methyl group rotation in the literature (when measured at spectrometers with similar resolution),[15,22] which indicates either additional dynamic mechanisms or different types of constraints for the motion that exist for this system. The second step of the elastic intensity at temperatures higher than the polymer T_g is caused by the polymer segmental motions, which become unfrozen above T_g. Above 420K, the elastic intensity of the polymer has dropped to values close to zero, indicating that all motions have become too fast for the experimental resolution of the specific instrument. The energy-resolved elastic intensity for the nanocomposite with 30wt% Hybrane exhibited a step-like decrease similar to the respective one of the polymer in the bulk for low temperatures, due to the insensitivity of the very local end- and/or side-group motion to the confinement.[22,45] For temperatures higher than the bulk polymer T_g, however, the elastic intensity does not drop to zero but shows a continuous decrease that is very similar for all wavevectors. This means that after all sub-T_g motions have relaxed, there is no motion within the experimental window at these temperatures; i.e., the segmental dynamics of the polymer

for some reason is suppressed for the polymer confined in the proximity of the inorganic surfaces within the galleries.

This behavior is reflected in the mean square displacement, $<u^2>$, extracted from the wavevector dependence of the elastically scattered intensity at each temperature according to Eq. 2. Figure 10 shows $<u^2>$ for the bulk polymer as a function of temperature as well as the respective $<u^2>$ for the layered silicate and the nanocomposite. The $<u^2>$ of the polymer is almost insensitive to temperature between 2-100K, it then weakly increases as the sub-T_g dynamic motions set in, it reaches a plateau and then it increases abruptly above the polymer T_g, when the segmental motion becomes active. The $<u^2>$ of the inorganic material is quite small and almost constant throughout the whole temperature range. The corresponding mean square displacement of the hybrid shows an initial increase that is very similar to that of the polymer following the same temperature dependence at low temperatures. For temperatures above the bulk polymer T_g, however, the $<u^2>$ does not show any further increase but remains almost constant indicating the absence of any dynamics within the experimental time window of IN10; this indicates that very few, if any, protons participate in the segmental motion of the confined polymer and leads to the conclusion that the majority of the polymer segments must be immobilized onto the inorganic surfaces of the silicate.

Quasielastic measurements were performed both at temperatures below and above the polymer glass transition temperature to study the sub-T_g and the segmental motions.[55] For all temperatures below T_g (not shown), the incoherent structure factor, $S(q,\omega)$, data for both the bulk Hybrane and the Hybrane nanocomposite show a quasi-elastic broadening that is independent of the wavevector, thus, corresponding to a very local motion; one could identify this as the motion of the methyl and/or the hydroxyl groups of the Hybrane molecules. The extracted relaxation times are, thus, wavevector independent whereas they exhibit Arrhenius temperature dependence, $\tau = \tau_0 \exp[E/RT]$, with activation energy of $E=0.49\pm0.25$ kJ/mol, which is very much smaller than the values quoted for methyl rotation in other polymer systems.[22] This difference in the behavior was attributed to the fact that methyls closer to the molecule core are less mobile than methyls at the end of the branches whereas the hydroxyl end groups, contributing to the dynamics at these temperatures as well, may participate in hydrogen bonds formed between groups of the same (intramolecular) or of neighboring molecules (intermolecular); the constraints due to the network of hydrogen bonds may influence not only the motion of the hydrogens of the hydroxyl groups but, even more importantly, may hinder the motion of the methyl groups.[55,145,147] The dynamics observed in

the nanocomposites (not shown) show similar behavior with that of the bulk polymer verifying the local character of the process; nevertheless they are somewhat faster, a fact that can be attributed to a reduced number of hydrogen bonds that can be formed under confinement, since the molecules do not have the space to retain all possible bulk conformations.

The incoherent structure factor $S(q,\omega)$ for the bulk polymer was measured at temperatures higher than the polymer T_g,[55] as well, i.e., at temperatures above 330K. Figure 11a shows the temperature dependence of the $S(q,\omega)$ for a specific wavevector together with the analysis of the experimental data for each temperature with the elastic and quasielastic contributions; the broadening of the wings of $S(q,\omega)$ with temperature that is accompanied by a drop of the elastic intensity is evident. The $S(q,\omega)$ for Hybrane at 390K for various wavevectors is shown in Figure 11b; a strong wavevector dependence is observed with the total as well as the elastic intensity decreasing with increasing wavevector. At the same time molecular dynamics simulations were performed, in order to assist the interpretation of the QENS data, and the intermediate incoherent structure factor $S(q,t)$ was calculated over a six orders of magnitude time-window (~10fs to ~10ns) for wavevectors similar to those examined by QENS.[55] Three processes were evident in the distribution of relaxation times; one at the ps-timescale, which gains amplitude as q increases, a second peak of lower amplitude extending from 10ps to 100ps, which shows no significant dependence of its amplitude on q, and a slower process at the ns-timescale, which loses amplitude upon increasing wavevector (i.e., upon decreasing the examined length-scale). The fast process is related to a very fast tumbling motion of the bond through which a hydrogen atom is attached to the backbone, to a methyl or to a hydroxyl group, whereas the slower is associated with the segmental relaxation. The intermediate process is correlated to a process that is intimately related to a motion involving the polymer branches.[55]

Figure 12 shows the wavevector dependencies of the average relaxation times obtained from the analysis of the experimentally measured $S(q,\omega)$ of Hybrane (Figure 11a,b) at temperatures above T_g as well as from the analysis of the calculated $S(q,t)$.[55] The relaxation times obtained from the simulation show different wavevector dependencies with the slower segmental relaxation exhibiting the stronger one. The experimentally measured τ_{ave} values lie between the intermediate and the slow processes of the simulation, whereas they exhibit different wavevector dependencies and show an apparent peculiar temperature dependence. Comparison of these times to the respective ones from molecular dynamics simulations leads

to the conclusion that, at the lower temperatures above T_g, the observed process is influenced by both the intermediate and slow processes predicted by simulations and it is only at the two highest temperatures that both the relaxation times and their wavevector dependence indicate that the pure segmental relaxation is indeed observed.[55]

Figure 11c shows the experimental $S(q,\omega)$ for the nanocomposite over a broad range of temperatures above the T_g of the bulk polymer. Nevertheless, further than a decrease of the elastic intensity as a function of temperature, there is no quasi elastic broadening. The data do not show any temperature dependence even at the highest temperature measured and all spectra almost coincide with the instrumental resolution function, indicating frozen dynamics at least for the experimental time range accessible by IN10. This result illustrates the effect of both the confinement and the Hybrane/Na$^+$MMT interactions on polymer dynamics. This agrees with previous works, where slower dynamics was observed when strong attractive interactions exist between the polymer and the solid surfaces,[52,76,149,150] as well as with works that obtained a reduction of free volume with the incorporation of layered silicates in polypropylene and polystyrene nanocomposites due to the "solidification" on the clay platelets.[151,152]

In order to investigate whether the slower dynamics under confinement is found in other hyperbranched systems as well, and at the same time to extend the time interval of the experimental measurements, the Boltorn H20, H30 and H40 polymers and their Na$^+$-MMT hybrids with 50wt% polymer were studied by dielectric spectroscopy.[57] Figure 13 shows representative spectra for three temperature pairs, below, slightly above and much above the T_g of the second generation hyperbranched polymer, Boltorn H20, in the bulk and for the respective 50 wt% nanocomposite, together with their analysis utilizing multiple relaxation processes expresses with Havriliak-Negami functions. At low temperatures below T_g, a very broad peak covering almost seven orders of magnitude in frequency is observed (Figure 13a), which shifts to higher frequencies as temperature increases. This is analyzed utilizing two sub-T_g relaxation processes attributed to the motion of hydroxyl groups and/or the orientation fluctuations of the ester groups, the so called γ- and β-processes, respectively, according to the literature.[137,138,140] All three generations of the hyperbranched polyester polyols investigated, exhibit this broad peak at temperatures below 283K showing very similar characteristics. At temperatures around the T_g of each polymer, another process appears related to the glass transition dynamics (α-process) as identified by the quantitative analysis (Figures 13c and 13e). At even higher temperatures (333-363K, depending on the generation)

the observation of any relaxation processes is partially obscured by a dc conductivity contribution for all the three polymers.

In the case of the nanocomposites, measurements were performed over a much broader temperature range than the respective polymers both from the low and the high temperature regime. Clear differences are observed in the spectra of the hybrids compared with the ones of bulk polymers both below and above the T_g of the bulk polymers. At low temperatures (Figure 13b), the spectra seem to have multiple relaxation processes like in the case of the pure polymer; however, all curves have a very different shape, lower dielectric strength and significantly faster relaxation times (when compared at the same temperature). For higher temperatures, but still below the bulk polymer T_g, the presence of another process becomes evident (Figure 13d) whereas for even higher temperatures (above 300K), an additional process appears (Figure 13f), which was not present in the neat polymers either because it was obscured by conductivity or because it indeed exists only in hybrids due to either the confinement or to the presence of the surfaces.

The relaxation times of all processes obtained from the analysis of the experimental spectra are shown in Figure 14 in an Arrhenius representation. The relaxation times of the γ-process almost coincide for the three hyperbranched polymers in the bulk (Figure 14a) and follow an Arrhenius temperature dependence, $\tau = \tau_0 \exp[E/RT]$, with activation energy $E_\gamma \approx$ 67.0±2.0 kJ/mol (R is the gas constant). This process due to local fluctuations and rotations of the hydroxyl groups exhibits an activation energy that is lower than the ones reported in the literature[137,138,140] but still high in comparison to local processes of linear polymers.[45] The intermediate β-process can be clearly analyzed for few temperatures since it is in close proximity to the other two processes as temperature increases. It follows Arrhenius temperature dependence with activation energy $E_\beta \approx 79\pm8$ kJ/mol that may depend slightly on the generation. For the segmental α-process, a clear dependence on the generation is observed in accordance with the differences in the T_g's of each polymer. Moreover, the temperature dependence of this process appears to conform to the Vogel-Fulcher-Tammann equation.

The nanocomposites exhibit a different dynamic behavior for both the sub-T_g processes and the segmental dynamics. Figure 14b shows the relaxation times of the different modes present for all nanohybrids. The relaxation times of the two sub-T_g processes, which exist in the nanocomposites as well, are much faster than the respective ones of the neat polymers and exhibit much weaker Arrhenius temperature dependencies. On the other hand,

both processes have very similar relaxation times when the three confined polymers are compared. For the fastest process, named γ', an average activation energy of $E_{\gamma'} \approx 29\pm5$ kJ/mol can be determined, which is much lower than the one of the bulk polymers but very similar to that obtained for the sub-T_g process for a linear PEO investigated with dielectric spectroscopy.[45] The second sub-T_g process, named β', shows a similar temperature dependence with the γ' with average activation energy for the three Boltrons being $E_{\beta'} \approx 27\pm5$ kJ/mol. The high activation energies of the corresponding γ and β processes for the Boltorns in the bulk, identified as the motion of the polar hydroxyl and carbonyl groups, are attributed to the constraints to the motion imposed by the hydrogen bond network formed. Under confinement, the flatten conformation that the polymers possess due to the spatial restrictions apparently limit the formation of the hydrogen bond network, thus, causing the activation energies for the respective motions to be lower than those in the bulk and to approach the values obtained for a non-hydrogen bonded system. At higher temperatures, even more significant differences in the behavior between the bulk polymers and the nanohybrids exist. Firstly, there is an intermediate process that emerges at temperatures much below the bulk polymer T_g, with an Arrhenius temperature dependence. This behavior resembles the α'-process, observed in previous studies on PMPS[40] and PEO[45] under confinement. In the case of the Boltorns, the α'-process is much faster than the dynamics of the bulk polymers for low temperatures or in the proximity of the bulk T_g but, at higher temperatures, it appears to cross the α-process of the bulk polymer becoming significantly slower. The α'-process being the segmental motion modified due to the severe confinement shows very similar behavior for the three confined polymers with an activation energy of $E_{\alpha'} \approx 100\pm1$ kJ/mol. Moreover, the α'-process exhibits a significant dependence on the generation and appears at higher temperatures with increasing generation, following the changes in the bulk T_g's. At even higher temperatures, a slow process appears, for all confined systems, probably due to interfacial polarization due to the large number of interfaces constituting the nanocomposites and the ions trapped in their proximity. This process shows Arrhenius temperature dependence and a significant effect on the generation as well.

IV. Concluding Remarks

In this highlight article, we made an attempt to review investigations on the static and dynamic behavior of polymers when they are severely confined between the layers of inorganic layered silicates and to compare it with the respective behavior in the bulk. We have utilized an organophilic polymer, poly(methyl phenyl siloxane), mixed with organoclays and a hydrophilic linear poly(ethylene oxide) and hydrophilic hyperbranched polymers with different number and kind of functional groups mixed with hydrophilic Na-activated montmorillonite in order to vary the interactions between the polymer and the surfaces. In all cases, we were interested in achieving the formation of intercalated structures with ~1nm of severely confined polymer films residing within the galleries.

The polymer dynamics in confinement versus that in the bulk was probed by dielectric relaxation spectroscopy and quasielastic neutron scattering with energy-resolved elastic scattering scans as a function of temperature complementing the incoherent structure factor measurements. The techniques are able to identify both very local sub-T_g motions, related to the motion of side and/or end groups, as well as the segmental α-relaxation processes, related to glass transition dynamics, for the various systems.

Similarities and differences were identified in the behavior that depend on the length scale of the probed motion as well as on the polymer-inorganic surface interactions. The local sub-T_g processes were found to be mostly unaffected by the strong confinement. However, when such processes are influenced in the bulk by topological restrictions imposed by, e.g., a possible hydrogen bond network, these processes are significantly modified in confinement most probably because the hydrogen bond network is altered in the confined systems. The segmental motion was found, in all cases, to become faster under confinement exhibiting Arrhenius temperature dependence and being observed even below the glass transition of the bulk polymers, reflecting a reduced cooperativity under confinement.

The investigation of the effect of confinement on polymer glass transition and the respective dynamics is still an unresolved problem in the field of soft condensed matter. A plethora of complex materials from multi-component polymer systems to polymer nanocomposites that are utilized in a variety of applications can be affected by multiscale confinement effects. On the other hand, the development of smaller-and-smaller devices brings the relevant material length scales to sizes comparable or even smaller than the size of a few polymer segments. Understanding the behavior is a key point to designing the right polymeric system and tailoring its properties. A crucial parameter is the confining length and

how the structure, properties and dynamics depend on it. In all the cases presented in the present manuscript, the confining length was the same, defined by the intercalated structure of the polymers within the clays (the existence of an intercalated structure is, of course, determined by the polymer-surface interactions). Thus, systems with a changing confining length may help in this aspect; this can be achieved by utilizing polymer-(nano)particle nanocomposites where the confining length can be varied by changing the composition of the nanocomposites. Note, however, that in those cases, achieving confining lengths of the order of 1-2 nanometers is not possible. Furthermore, the effect of the severe confinement on the overall motion of a polymer chain has not been investigated in a significant extent. Even more, the effect of confinement on polymer structure and morphology is a matter of current research efforts as well.

Acknowledgements

30

References and Notes

1   M. D. Ediger, *Annu.Rev.Phys. Chem.*, 2000, **51**, 99-128.

2   S. C. Glotzer, *J. Non-Cryst. Solids,* 2000, **274**, 342-355.

3   R. Zorn, *J. Phys.: Condens. Matter,* 2003, **15**, R1025-R1046.

4   A. Arbe, *Physica B,* 2004, **350**, 178-185.

5   W. Paul and G. D. Smith, *Rep. Prog. Phys.,* 2004, **67**, 1117-1185.

6   D. Richter, M. Monkenbusch, A. Arbe and J. Colmenero, *Adv. Polym. Sci.,* 2005, **174**, 1-221.

7   J. Baschnagel and F. Varnik, *J. Phys: Condens. Matter,* 2005, **17**, R851-R953.

8   V. G. Sakai and A. Arbe, *Curr. Opin. Colloid Interface Sci.,* 2009, **14**, 381–390.

9   H. N. Lee, K. Paeng, S. F. Swallen and M. D. Ediger, *Science,* 2009, **323**, 231-234.

10   K. Chen, E. J. Saltzman and K. S. Schweizer, *J. Phys.-Cond. Matt.,* 2009, **21**, 503101.

11   J. L. Barrat, J. Baschnagel and A. Liulin, *Soft Matter,* 2010, **6**, 3430-3446.

12   J. Colmenero and A. Arbe, *J. Polym. Sci., Part B: Polym Phys.,* 2013, **51**, 87-113.

13   B. Frick and D. Richter, *Science,* 1995, **267**, 1939-1945.

14   J. Colmenero, A. J. Moreno and A. Alegria, *Prog. Polym. Sci.,* 2005, **30**, 1147-1184.

15   B. Frick and L. J. Fetters, *Macromolecules,* 1994, **27**, 974-980.

16   F. Alvarez, A. Alegria, J. Colmenero, T. M. Nicholson and G. R. Davies, *Macromolecules,* 2000, **33**, 8077-8084.

17   R. Zorn, B. Frick, and L. J. Fetters, *J. Chem. Phys.,* 2002, **116**, 845-853.

18   V. Arrighi, J. S. Higgins, A. N. Burgess and W. S. Howells, *Macromolecules,* 1995, **28**, 2745-2753.

19   C. Chen, J. K. Maranas and V. Garcia-Sakai, *Macromolecules,* 2006, **39**, 9630-9640.

20   A. Arbe, J. Colmenero, B. Frick, M. Monkenbusch and D. Richter, *Macromolecules,* 1998, *3***1**, 4926-4934.

21   K. Karatasos, J.-P. Ryckaert, R. Ricciardi, F. Laupretre, *Macromolecules,* 2002, **35**, 1451-1462.

22   K. Chrissopoulou, S. H. Anastasiadis, E. P. Giannelis and B. Frick, *J. Chem. Phys.,* 2007, **127**, 144910.

23   S. H. Anastasiadis, K. Chrissopoulou and B. Frick, *Mater. Sci. Eng. B,* 2008, **152**, 33-39.

24   M. Bée, *Quasielastic Neutron Scattering: Principles and Applications in Solid State Chemistry, Biology and Materials Science*; Adams Hilger: Bristol, U.K., 1988.

25   J. Mijovic, X. Y. Chen, and J. W. Sy, *Macromolecules,* 1999, **32**, 5365-5374.

26   A. De La Rosa, L. Heux and J. Y. Cavaille, *Polymer,* 2001, **42**, 5371-5379.

27   C. Hakme, I. Stevenson, L. David, G. Bolteux, G. Seytre and A. Schonhals*, J. Non-Cryst Sol.,* 2005, **351**, 2742-2752.

28   I. Quintana, A. Arbe, J. Colmenero and B. Frick, *Macromolecules,* 2005, **38**, 3999-4013.

29   S. Arrese-Igor, A. Arbe, A. Alegria, J. Colmenero and B. Frick, *J. Chem Phys.,* 2004, **120**, 423-436.

30   G. Meier, F. Fujara and W. Petry, *Macromolecules,* 1989, **22**, 4421-4425.

31   J. E. Forrest and R. A. L. Jones, *Polymer Surfaces, Interfaces and Thin Films*; A. Karim, S. Kumar, Eds.; World Scientific: Singapore, 2000.

32   J. A. Forrest and K. Dalnoki-Veress, *Adv. Colloid Interface Sci.* 2001, **94**, 167-196.

33   P. A. O'Connel and G. B. Mc Kenna, *Science,* 2005, **307**, 1760-1763.

34   Special Issue on "Progress in Dynamics in Confinement", R. Zorn, L. van Eijck, M. M. Koza and B. Frick Eds. [*Eur. Phys. J.-Sp. Top.,* 2010, **189**, 1-302]. G. B. McKenna, *Europ. Phys. J.-Sp. Top.* 2010, **189**, 285-302.

35   J. M. Zanotti, K. Lagrene, N. Malikocova, P. Judeinstein, K. Panesar, J. Ollivier, S. Rols, M. Mayne-L'Hermite, M. Pinault and P. Boulanger, *Eur. Phys. J.-Sp.Top.,* 2012, **213**, 129-148.

36   H. K. Nguyen, M. Labardi, S. Capaccioli, M. Lucchesi, P. Rolla, D. Prevosto, *Macromolecules,* 2012, **45**, 2138-2144.

37   S. Perkin, J. Klein, *Soft Matter*, 2013, **9**, 10438-10441.

38   E. U. Mapesa, M. Tress, G. Schulz, H. Huth, C. Schick, M. Reiche, F. Kremer, *Soft Matter*, 2013, **9**, 10592-10598.

39   A. Bansal, H. Yang, C. Li, K. Cho, B. C. Benicewicz, S. K. Kumar, L. S. Schadler, *Nature Mater.,* 2005, **4**, 693-698.

40   S. H. Anastasiadis, K. Karatasos, G. Vlachos, E. Manias, E. P. Giannelis, *Phys. Rev. Lett.,* 2000, **84**, 915–918.

41   S. H. Anastasiadis, *J. Phys. IV France*, 2000, **10**, 255-258.

42   B. J. Ash, R. W. Siegel, and L. S. Schadler, *J. Polym. Sci., Part B: Polym. Phys.,* 2004, **42**, 4371-4383.

43   B. Frick, C. Alba-Simionesco, G. Dosseh, C. Le Quellec, A. J. Moreno, J. Colmenero, A. Schonhals, R. Zorn, K. Chrissopoulou, S. H. Anastasiadis and K. Dalnoki-Veress, *J. Non-Cryst. Sol.,* 2005, **351**, 2657-2667.

44   A. Schoenhals, H. Goering, Ch. Schick, B. Frick and R. Zorn, *J. Non-Cryst. Sol.,* 2005, **351**, 2668–2677.

45   M. M. Elmahdy, K. Chrissopoulou, A. Afratis, G. Floudas and S. H. Anastasiadis, *Macromolecules,* 2006, **39**, 5170-5173.

46   K. Chrissopoulou, A. Afratis, S. H. Anastasiadis, M. M. Elmahdy and G. Floudas, *Europ. Phys. J.-Sp. Top.,* 2007, **141**; 267-271.

47   J. M. Kropka, V. Pryamitsyn, and V. Ganesan, *Phys. Rev. Lett.,* 2008, **101**, 075702.

48   A. Schoenhals, H. Goering, Ch. Schick, B. Frick, M. Mayorova and R. Zorn, *Eur. Phys. J. Sp. Top.,* 2007, **141**, 255–259.

49   S. K. Kumar and R. Krishnamoorti, *Ann. Rev. Chem. Biomol. Eng.,* 2010, **1**, 37-58.

50   P. Rittigstein, R. D. Priestley, L. J. Broadbelt and J. M. Torkelson, *Nature Mater.,* 2007, **6**, 278-282.

51   C. Zhang, Y. Guo and R. D. Priestley, *Macromolecules,* 2011, **44**, 4001-4006.

52   L. T. Vo, S. H. Anastasiadis and E. P. Giannelis, *Macromolecules,* 2011, **46**, 6162-6171.

53   F. Barroso-Bujans, F. Fernandez-Alfonso, S. Cerveny, S. F. Parker, A. Alegria and J. Colmenero, *Soft Matter,* 2011, **16**, 7173-7176.

54   F. Barroso-Bujans, S. Cerveny, A. Alegria and J. Colmenero, *Macromolecules,* 2013, **46**, 7932-7939.

55   S. Fotiadou, C. Karageorgaki, K. Chrissopoulou, K. Karatasos, I. Tanis, D. Tragoudaras, B. Frick and S. H. Anastasiadis, *Macromolecules,* 2013, **46**, 2842-2855.

56   S. Alexandris, G. Sakellariou, M. Steinhart and G. Floudas, *Macromolecules,* 2014, **47**, 3895-3900.

57   K. Androulaki, K. Chrissopoulou, D. Prevosto, M. Labardi and S. H. Anastasiadis, *ACS Appl. Mater. Inter.,* 2014, DOI 10.1021/am507571y.

58   T. J. Pinnavaia and G. W. Beall, *Polymer-Clay Nanocomposites*; John Wiley & Sons, West Sussex, 2000.

59   E. P. Giannelis, R. Krishnamoorti and E. Manias, *Adv. Polym. Sci.,* 1999, **138**, 107-147.

60   M. Alexandre and P. Dupois, *Mat. Sci. and Eng. R*, 2000, **28**, 1-63.

61   S. Sinha Ray and M. Okamoto, *Prog. Polym. Sci.*, 2003, **28**, 1539-1641.

62   S. C. Tjong, *Mater. Sci. Eng. R*, 2006, **53**, 73-197.

63   K. Chrissopoulou, I. Altintzi, S. H. Anastasiadis, E. P. Giannelis, M. Pitsikalis, N. Hadjichristidis and N. Theophilou, *Polymer* 2005, **46**, 12440-12451.

64   K. Chrissopoulou, I. Altintzi, I. Andrianaki, R. Shemesh, H. Retsos, E. P. Giannelis and S. H. Anastasiadis, *J. Polym. Sci. Part B: Polym. Phys.,* 2008, **46**, 2683-2695.

65   K. Chrissopoulou and S. H. Anastasiadis, *Eur. Polym. J.,* 2011, **47**, 600-613.

66   R. A. Vaia, B. B. Sauer, O. K. Tse and E. P. Giannelis, *J. Polym. Sci. Part B: Polym. Phys.*, 1997, **35**, 59-67.

67   E. Hackett, E. Manias and E. P. Giannelis, *Chem. Mater.,* 2000, **12**, 2161-2167.

68   Z. Shen, G. P. Simon and Y. Cheng, *Eur. Polym. J.*, 2003, **39**, 1917-1924.

69   R. A. Vaia, K. D. Jandt, E. J. Kramer and E. P. Giannelis, *Chem. Mater.*, 1996, **8**, 2628-2635.

70   R. A. Vaia, K. D. Jandt, E. J. Kramer and E. P. Giannelis, *Macromolecules*, 1995, **28**, 8080-8085.

71   A. Usuki, Y. Kojima, M. Kawasumi, A. Okada, Y. Fukusihima, T. T. Kurauchi, and O. Kamigaito, *J. Mater. Res.*, 1993, **8**, 1179-1184.

72   K. Chrissopoulou, K. S. Andrikopoulos, S. Fotiadou, S. Bollas, C. Karageorgaki, D. Christofilos, G. A. Voyiatzis and S. H. Anastasiadis, *Macromolecules,* 2011, **44**, 9710-9722.

73   H. Papananou, S. Fotiadou, K. Chrissopoulou and S. H. Anastasiadis, *Mater. Sci. Forum*, 2012, **714**, 85-90

74   M. Bohning, H. Goering, A. Fritz, K.-W. Brzezinka, G. Turky, A. Schonhals and B. Schartel, *Macromolecules,* 2005, **38**, 2764-2774.

75   S. Fotiadou, K. Chrissopoulou, B. Frick and S. H. Anastasiadis, *J. Polym. Sci., Part B: Polym. Phys.,* 2010, **48**, 1658-1667.

76   C. Lorthioir, F. Laupretre, J. Soulestin and J. M. Lefebvre, *Macromolecules,* 2009, **42**, 218-230.

77   D. Prevosto, M. Lucchesi, M. Bertoldo, E. Passaglia, F. Ciardelli and P. Rolla, *J. Non-Cryst. Sol.,* 2010, **356**, 568–573.Goering

78   M. Labardi, D. Prevosto, K. H. Nguyen, S. Capaccioli, M. Lucchesi and P. Rolla, *J. Vac. Sci. Technol. B,* 2010, **28**, C4D11-17.

79   K. L. Ngai, *Philos. Mag. B,* 2002, **82**, 291–303

80   C. Mischler, J. Baschnagel and K. Binder, *Adv. Colloid. Interf. Sci.,* 2001, **94**, 197-227.

34

81   J. S. Higgins and H. C. Benoit, *Polymers and Neutron Scattering*, Oxford University Press, New York 1994.

82   M. Doxastakis, K. Chrissopoulou, A. Aouadi, B. Frick, T. P. Lodge and G. Fytas, *J. Chem. Phys.,* 2002, **116**, 4707-4714.

83   J. P. Runt and J. J Fitzgerald, *Dielectric spectroscopy of polymeric materials: fundamentals and applications*, Am. Chem. Soc. Washington, DC, 1997.

84   A. Schonhals and F. Kremer, *Broadband Dielectric Spectroscopy,* Springer Berlin Heidelberg, 2003.

85   K. Karatasos, S. H. Anastasiadis, A. N. Semenov, G. Fytas, M. Pitsikalis and N. Hadjichristidis, *Macromolecules*, 1994, **27**, 3543-3552.

86   S. Provencher, *Comp. Phys. Comm.,* 1982, **27**, 229-242.

87   A. Schoenhals, C. Schick, H. Huth, B. Frick, M. Mayorova and R. Zorn, *J. Non-Cryst. Sol.*, 2007, **353**, 3853-3861.

88   M. Paluch, R. Casalini, A. Patkowski, T. Pakula and C. M. Roland, Phys. Rev. E, 2003, **68**, 031802.

89   H. Kriegs, J. Gapinski, G. Meier, M. Paluch, S. Pawlus and A. Patkowski, *J. Chem. Phys.,* 2006, **124**, 104901.

90   G. Fytas, Y.-H. Lin and B. Chu, *J. Chem. Phys.,* 1981, **74**, 3131-3138.

91   A. Schoenhals, H. Goering, Ch. Schick, B. Frick and R. Zorn, *Colloid Polym. Sci.*, 2004, **282**, 882-891.

92   Organophilized hectorite and montmorillonite were utilized. The organically modified layered silicates were prepared by a cation exchange reaction between the Na^+ in the hydrophilic sodium-activated silicate hosts and dioctadecyl-dimethyl-ammonium bromide at exchange capacity, in order to render the originally hydrophilic silicate surface organophilic.

93   The poly(methyl phenyl siloxane) homopolymer, PMPS, with molecular weight M_w = 2,600 g/mol, polydispersity index M_w/M_n=1.2 and glass transition temperature T_g=223K was purchased from Aldrich. PMPS is a hydrophobic polymer that interacts favorably only with organophilized layered silicates.

94   R. C. Reynolds, *Reviews in Mineralogy*; Post, DLBJE Ed.; The Mineralogical Society of America: Washington DC, 1989; Vol. 20; pp 145-183.

95   A. Kiersnowski, K. Kolman, I. Lieberwirth, S. Yordanov, H.-J. Butt, M. R. Hansen and S. H. Anastasiadis, *Soft Matter*, 2013, **9**, 2291-2301.

96   D. Boese, B. Momper, G. Meier, F. Kremer, J.-U. Hagenah and E. W. Fischer, *Macromolecules*, 1989, **22**, 4416-4421.

97   A. Schoenhals, H. Goering, Ch. Schick, B. Frick and R. Zorn*, Eur. Phys. J. E*, 2003, **12**, 173-178.

98   A. Schoenhals, H. Goering, K. W. Brzezinka and Ch. Schick, *J. Phys: Cond. Matt.*, 2003, **15**, S1139-S1148.

99   E. Ruiz-Hitzky, *Adv. Mater.,* 1993, **5**, 334-340.

100   R. A. Vaia, S. Vasudevan, W. Krawiec, L. G. Scanlon and E. P. Giannelis, *Adv. Mater.,* 1995, **7**, 154-156.

101   S. Wong, S. Vasudevan, R. A. Vaia, E. P. Giannelis and D. B. Zax, *J. Am. Chem. Soc.,* 1995, **I17**, 7568-7569.

102   S. Wong, R. A. Vaia, E. P. Giannelis and D. B. Zax, *Sol. Stat. Ion.,* 1996, **86**, 547-557.

103   F. Croce, G. B. Appetecchi, L. Persi and B. Scrosati, *Nature,* 1998, **394**, 456-459.

104   J. Zhang, H. Han, S. Wu, S. Xu, Y. Yang, C. Zhou and X. Zhao, *Sol. Stat. Ion.,* 2007, **178**, 1595-1601.

105   H. C. Zhang, Y. Zhao, J. Wang and H. Zheng, *J. Phys. Chem. C,* 2007, **111**, 5382-5388.

106   A. Kelarakis and E. P. Giannelis, *Polymer,* 2011, **52**, 2221-2227.

107   R. Krishnamoorti, R. A. Vaia and E. P. Giannelis, *Chem. Mater.*, 1996, **8**, 1728-1734.

108   K. Lagrene, J. M. Zanotti, M. Daoud, B. Farago and P. Judeinstein, *Europ. Phys. J. – Spec. Top.,* 2010, **189**, 231-237.

109   F. Barroso-Bujans, F. Fernandez-Alonso, S. Cerveny, S. Arrese-Igor, A. Alegria and J. Colmenero, *Macromolecules,* 2012, **45**, 3137-3144.

110   C. Lai, R. Ayyer, A. Hiltner and E. Baer, *Polymer*, 2010, **51**, 1820-1929.

111   Y. Miwa, A. R. Drews, and S. Schlick, *Macromolecules*, 2008, 41, 4701-4708.

112   V. Kuppa, S. Menakanit, R. Krishnamoorti and E. Manias, *J. Polym Sci: Part B: Polym. Phys.*, 2003, **41**, 3285-3298.

113   V. Kuppa and E. Manias, *J. Chem. Phys.*, 2003, **118**, 3421-3429.

114   The poly(ethylene oxide) homopolymer, PEO, was purchased from Aldrich. Its molecular weight is 100,000 g/mol and its polydispersity index is $M_w/M_n = 2.4$, as determined by size exclusion chromatography utilizing polystyrene standards. The polymer possesses hydroxyl chain ends and it exhibits a glass transition temperature T_g=206K and a melting temperature T_m=338K. Due to its polar character, this polymer is expected to intercalate within hydrophilic layered materials.

36

---

[115]   Hydrophilic sodium-activated montmorillonite, Na^+-MMT (Southern Clay) were utilized with a cation exchange capacity (CEC) of 92.6 mmol/100g. It was used following heating at 120°C overnight in a vacuum oven to allow removal of excess water molecules from the hydrophilic galleries. The presence of hydrated Na^+ makes the galleries hydrophilic so that polar polymers can mix without the need of modification of the silicate hosts.

[116]   H. Tadokoro, Y. Chatani, T. Yoshihara, S. Tahara and S. Murahashi, *Macromol. Chem. Phys.,* 1964, **73**, 109-127.

[117]   Y. Takahashi, I. Sumita and H. Tadokoro, *J. Polym. Sci. Polym. Phys.,* 1973, **11**, 2113-2122.

[118]   E. Bortel, S. Hodorowicz and R. Lamot, *Macromol. Chem. Phys.,* 1979, **180**, 2491-2498.

[119]   C. Saujanya and S. Radhakrishnan, *J.Appl. Pol. Sci.,* 1997, **65**, 1127-1137.

[120]   G. Floudas, K. Mpoukouvalas and P. Papadopoulos, *J. Chem. Phys.,* 2006, **124**, 074905.

[121]   C. M. Roland, S. Hensel-Bielowka, M. Paluch, and R. Casalini, *Rep. Prog. Phys.,* 2005, **68**, 1405-1478.

[122]   K. L. Ngai and C. M. Roland, *Macromolecules,* 1993, **26**, 6824-6830.

[123]   K. L. Ngai, *J. Non Cryst. Sol.*, 2007, **353**, 4237-4235

[124]   K. Chrissopoulou, S. Fotiadou, B. Frick and S. H. Anastasiadis, *Macromol. Symp.*, 2013, **331-332**, 50-57.

[125]   S. Fotiadou, A. Afratis, K. Chrissopoulou, B. Frick and S. H. Anastasiadis, in preparation.

[126]   D. A. Tomalia, *Mater. Today,* 2005, **8**, 35-46.

[127]   D. Yan, C. Gao and H. Frey, *Hyperbarnched Polymers : Synthesis, Properties and Applications.* Wiley Series on Polymer Engineering and Technology, 2011.

[128]   D. Konkolewicz, M. J. Monteiro and S. Perrier, *Macromolecules,* 2011, **44**, 7067-7087.

[129]   D. A. Tomalia, *Twenty-first Century Polymer Science After Staudinger: The Emergence of Dendrimers/Dendritic Polymers as a Fourth Major Architecture and Window to a New Nano-periodic System*, Percec, V. Eds. *Adv. Polym. Sci.* 2013, **261**, 321-389.

[130]   B. I. Voit, A. Lederer, *Chem. Rev.,* 2009, **109**, 5924–5973.

[131]   D. Ratna, R. Varley and G. P. Simon, *J. Appl. Polym. Sci.,* 2004, **92**, 1604–1610.

[132]   J. Zou, Y. Zhao and W. Shi, *J. Membr. Sci.* 2004, **245**, 35–40.

133   X. Wang, H. Liu and Y. Jin, *J. Phys. Chem. B,* 2006, **110**, 10236–10240.

134   B. Pettersson, *Pigment Resin Technol.,* 1996, **25**, 4–14.

135   R. Reul, J. Nguyen and T. Kissel, *Biomaterials,* 2009, **30**, 5815–5824.

136   I. Tanis, K. Karatasos, A. N. Assimopoulou and V. P. Papageorgiou, *Phys. Chem. Chem. Phys.,* 2011, **13**, 11808-11817.

137   E. Malmstrom, F. Liu, R. H. Boyd, A. Hult and U. W. Gedde, *Polym Bull.,* 1994, **3**2, 679-685.

138   E. Malmstrom, A. Hult, U. W. Gedde, F. Liu and R. H. Boyd, *Polymer,* 1997, **38**, 4873-4879.

139   P. W. Zhu, S. Zheng and G. Simon, *Macromol. Chem. Phys*., 2001, **202**, 3008-3017.

140   G. Turky, S. S. Shaaban and A. Schoenhals, *J. Appl.Polym. Sci.,* 2009, **113**, 2477–2484.

141   I. Tanis and K. Karatasos, *Phys. Chem. Chem. Phys.,* 2009, **11**, 10017–10028.

142   I. Tanis and K. Karatasos, *Macromolecules,* 2009, **42**, 9581–9591.

143   The polyester amide Hybrane S 1200 has a number-average molecular weight M_n = 1,200 g/mol and was supplied by DSM. Hybrane[144] is amorphous with a T_g of 315-320 K (DSM Hybrane Safety Data); its radius of gyration R_g, calculated utilizing Molecular Dynamics simulations, is 7.6Å at 350K.[145]

144   P. Froehling, *J. Polym. Sci., Part A: Polym. Chem.,* 2004, **42**, 3110-3115.

145   I. Tanis, D. Tragoudaras, K. Karatasos and S. H. Anastasiadis, *J. Phys. Chem. B,* 2009, **113**, 5356-5368.

146   The second, third and fourth generations of the polyester polyols Boltorn™ H20, H30 and H40, were supplied by Polymer Factory. These polymers are amorphous with their chains consist mainly of ester groups and hydroxyl end groups. Their molecular weights are M_n~1,750, 3,600 and 7,300 g/mol and their glass transition temperatures are 287, 308 and 319K, respectively.

147   E. Zagar, M. Huskin, J. Grdadolnik, M. Zigon and A. Zupancic-Valant, *Macromolecules,* 2005, **38**, 3933-3942.

148   E. Zagar, M. Huskic and M. Zigon, *Macromol. Chem. Phys.,* 2007, **208**, 1379-1387.

149   W. Xu, S. Raychowdhury, D. D. Jiang, H. Retsos and E. P. Giannelis, *Small,* 2008, **4**, 662–669.

150   M. Hernadez, J. Carretero-Gonzalez, R. Verdejo, T. A. Ezquerra, M. A.; Lopez-Manchado, *Macromolecules,* **2010**, *43*, 643–651.

38

151 A. M. Jamieson, B. G. Olson and S. Nazarenko, "Positron Annihilation Lifetime Studies of Free Volume in Heterogeneous Polymer Systems", In *Polymer Physics: from Suspensions to Nanocomposites and Beyond*, L. A. Utracki and A. M. Jamieson, Eds.; Wiley & Sons Inc., USA, 2010.

152 L. A. Utracki and R. Simha, *Macromolecules*, 2004, **37**, 10123-10133.

Figure Captions

1. X-ray diffractograms of the organophilized silicate and the nanocomposites with 15wt%, 20wt%, 25wt%, 30wt% and 70wt% PMPS content. The curves have been shifted vertically for clarity. Adopted from ref. 22 (with permission).

2. Arrhenius plot of the relaxation times for PMPS nanocomposites with 15wt% (triangles), 20wt% (circles), 25wt% (squares) and 30wt% (diamonds) PMPS. The processes are indicated as follows: α'- process (open symbols), intermediate process (open crossed symbols) and slow-bulk-like process (solid symbols). The segmental motion of bulk PMPS is represented with a solid line. The dash line is the VFT fit to the α' relaxation times. Reprinted from ref. 40 (with permission).

3. Elastic temperature scans for wavevectors q=0.43, 0.54, 0.65, 087, 1.25, 1.70 and 1.92Å^{-1} of (a) PMPS, (b) organophilized silicate and (c) the PMPS25 intercalated nanocomposite with 25wt% PMPS. All data are normalised to the lowest temperature at each wavevector. (d) Temperature dependence of the mean square displacement obtained from the wavevector dependence of the elastic scans for PMPS (■), organosilicate (▲) and the intercalated PMPS25 nanocomposite (◊).The solid line is the sum of the msd for the PMPS and the silicate. Figures (a), (b) and (c) were adopted from ref. 22 and Figure (d) from ref. 23(with permission).

4. (a) Incoherent structure factor, $S(q,\omega)$ of (○) PMPS and (●) PMPS25 intercalated nanocomposite with 25wt% PMPS at T=100K for q=1.1Å^{-1}. The dash line represents the instrumental resolution function measured at T=2K whereas the solid lines corresponds to the total fit with Eq.1 to the experimental data for PMPS and PMPS25. (b) Wavevector dependence of the average relaxation times for the methyl group rotation of PMPS for T=80K (Δ), T=100K (○) and T=120K (□) and of PMPS25 for T=100K (●). Adopted from refs. 22 and 23 (with permission).

5. X-ray diffraction patterns for the PEO/Na$^+$MMT nanocomposites with 30wt%, 50wt%, 70wt%, 80wt% and 90wt% PEO content together with the measurements of bulk PEO and Na$^+$-MMT. The curves have been shifted vertically for clarity. Adopted from refs. 45 and 72 (with permission).

6. Imaginary part of the electric modulus at T=203 K for the pure PEO (■) and the PEO/Na$^+$MMT composites with PEO content: 95% (Δ), 90% (○), 80% (∇), 70% (◊), 50% (◁) and 30% (▷). The arrows indicate the α-, α'- and β-processes. The processes

needed for the deconvolution of the spectra for the 70wt% PEO are shown with dash-dotted (β), dashed (α') and dotted (α) lines, whereas the solid lines are the summations of the processes (together with the conductivity at high temperatures, which is not shown). Adopted from ref. 45 (with permission).

7. Arrhenius relaxation map for the PEO/Na$^+$MMT nanocomposites with 30wt% (squares), 50wt% (inverted triangles), 70wt% (triangles) and 80wt% PEO (diamonds) together with the relaxation times of bulk PEO (circles). The β- (open symbols), the α'- (half-filled symbols) and the α-processes (solid symbols) are shown. The error bars are comparable to the size of the symbols. Adopted from ref. 45 (with permission).

8. (a) Elastic intensity as a function of temperature for PEO ($\circ$), silicate ($\square$) and a 30wt% PEO nanocomposite (Δ) at $q=1.29$Å^{-1}. All data are normalised to the lowest temperature. (b) Quasielastic spectra of PEO ($\circ$), Na$^+$-MMT ($\square$) and the 30wt%PEO hybrid (Δ) at $q=1.29$Å^{-1} for T=345K. The solid line is the total fit with Eq. 1 to the experimental data of the nanohybrid whereas the dash line is the instrumental resolution. Adopted from ref. 124 (with permission).

9. X-ray diffraction patterns for the Hybrane/Na$^+$MMT nanocomposite with 30wt% as well as the three Boltorn/Na$^+$MMT with 50wt% polymer content together with the measurements of pure Na$^+$-MMT. The curves have been shifted vertically for clarity. Adopted from refs. 55 and 57 (with permission).

10. Temperature dependence of the mean square displacement, $<u^2>$, for the Hybrane ($\circ$), the Na$^+$-MMT ($\square$) and the nanocomposite with 30% Hybrane (Δ). Reprinted from ref. 55 (with permission).

11. Incoherent structure factor $S(q,\omega)$ of (a) Hybrane at wavevector $q=1.45$Å^{-1} and at temperatures 330K ($\Diamond$), 350K (∇), 370K ($\circ$) and 390K (Δ), above the polymer T_g, and (b) Hybrane at T=390K for wavevectors $q = 0.86$Å^{-1} ($\Diamond$), 1.18Å^{-1} (∇), 1.45Å^{-1}(Δ), 1.68Å^{-1}($\circ$) and 1.96Å^{-1}($\square$). The lines represent the total fit (solid lines) together with the elastic (dotted lines) and the quasi-elastic (dashed lines) contributions to the spectra. The insets show the respective quasi-elastic part of the spectra for the same temperatures and wavevectors as in the main Figures. (c) Incoherent structure factor, $S(q,\omega)$, of the nanocomposite with 30% Hybrane for various temperatures above the bulk polymer T_g. The line is the instrumental resolution measured at temperature 2K. The y-axis is shown at 10% of the intensity of the data for the temperature of 350K. Reprinted from ref. 55 (with permission).

12. Wavevector dependence of the average relaxation times obtained from the QENS experiments at 330K, 370K and 390K (half-filled symbols) and from the molecular dynamics simulation (T=370K solid symbols, T=405K open symbols) at temperatures greater than the bulk polymer T_g. Reprinted from ref. 55 (with permission).

13. Imaginary part of the dielectric permittivity, $\varepsilon''(\omega)$, for the H20 (a, c, e) and for the H20 / Na$^+$-MMT with 50wt% polymer content (b, d, f) at 223 K (a, b; upper part), 293K (c, d) (middle part) and 303K (e) and 333K (f) (lower part). The processes needed for the deconvolution of the spectra are shown with dashed (γ and γ'), dotted (β and β'), dash-dotted (α and α') and dash-dot-dot (slow) lines, whereas the solid lines are the convolution of the processes (together with the conductivity at high temperatures). Reprinted from ref. 57 (with permission).

14. Arrhenius relaxation map for the (a) H20, H30, H40 hyperbranched polymers in the bulk and (b) for Boltorn/Na$^+$-MMT nanocomposites with 50wt% of the respective polymer. The processes are indicated as follows: the γ- and γ'- processes (filled symbols), the β- and β'-processes (half-filled symbols), the α- and α'- processes (open symbols) and the slow-processes (open crossed symbols). H20 (squares), H30 (circles) and H40 (diamonds). Reprinted from ref. 57 (with permission).
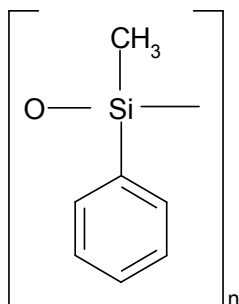
Scheme 1: Molecular structure of poly(methyl phenyl siloxane)
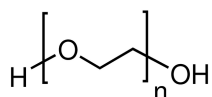
Scheme 2: Molecular structure of poly(ethylene oxide)
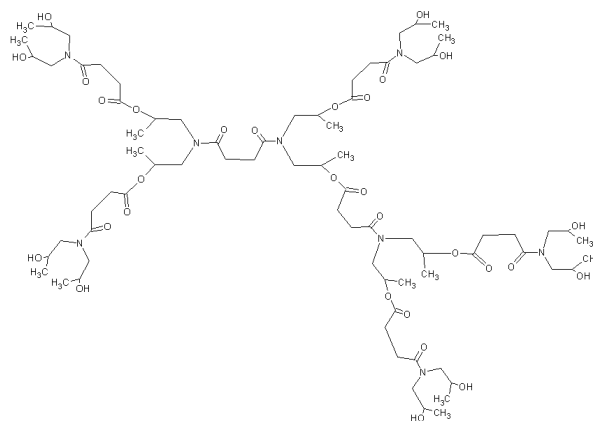
Scheme 3: Molecular structure of hyperbranched poly(ester amide) Hybrane
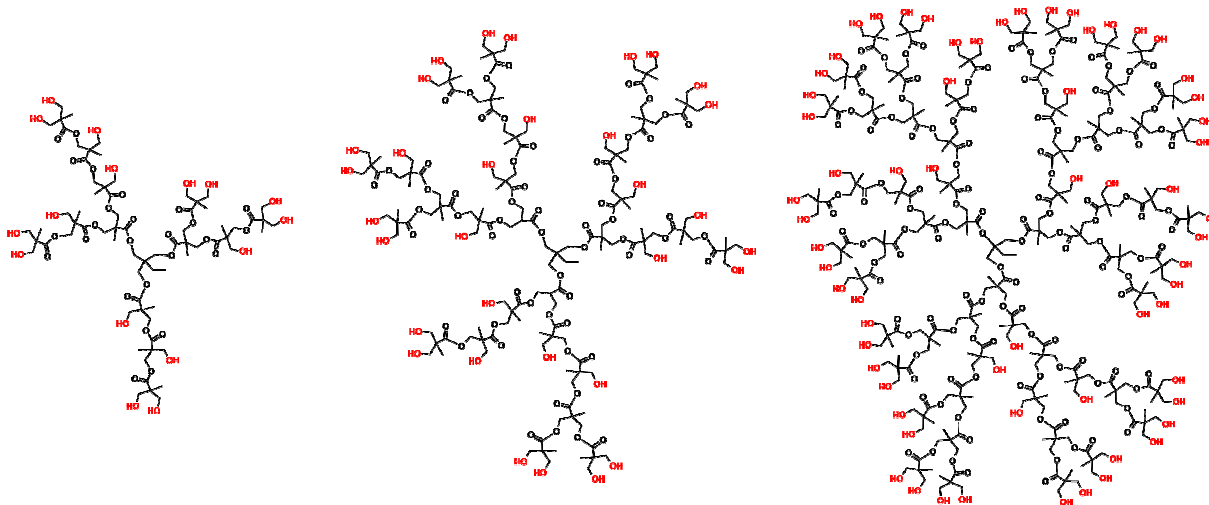
Scheme 4: Molecular structures of the three generations of hyperbranched polyerster polyols Boltorn
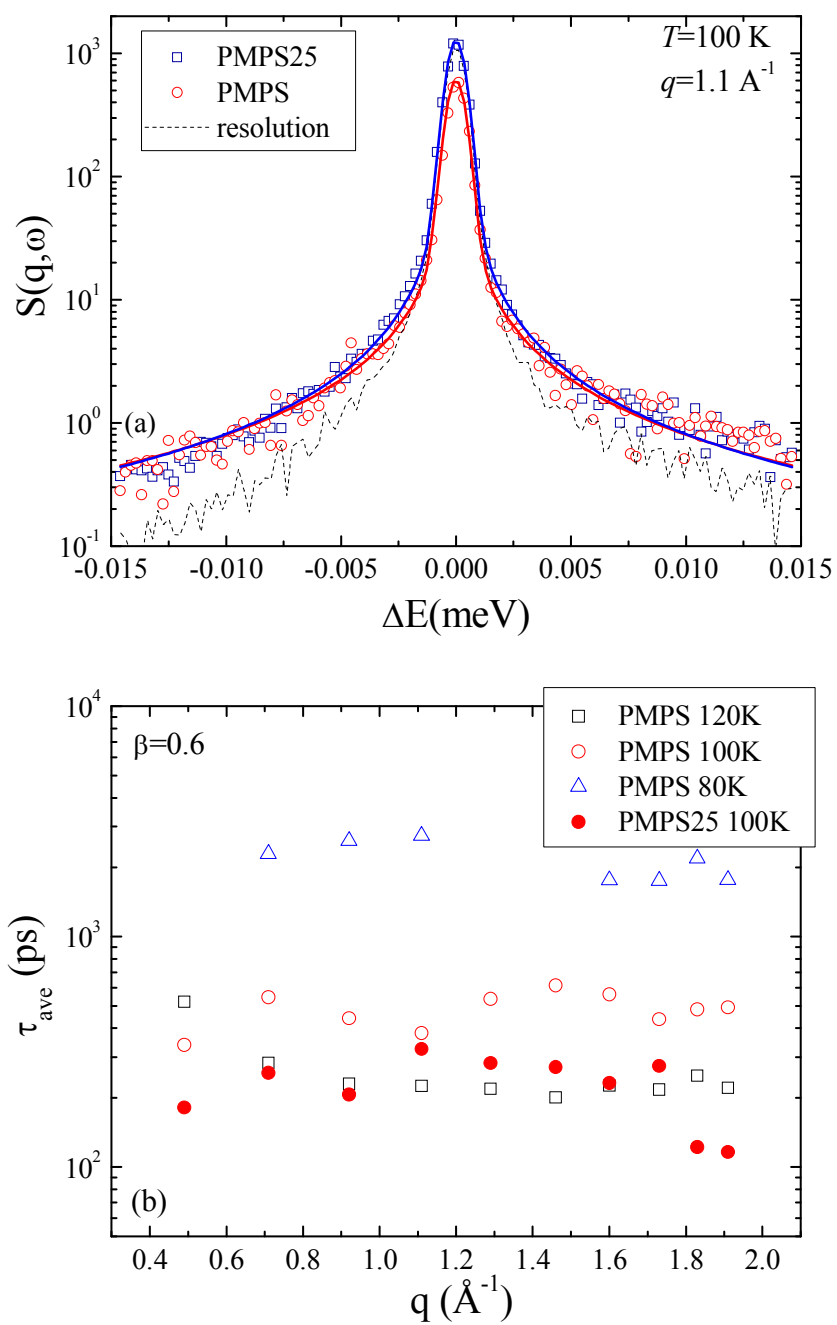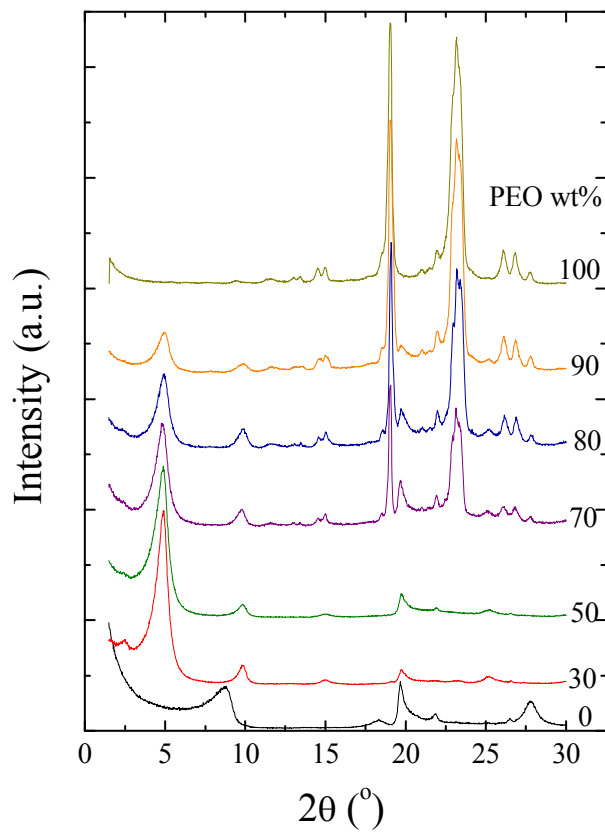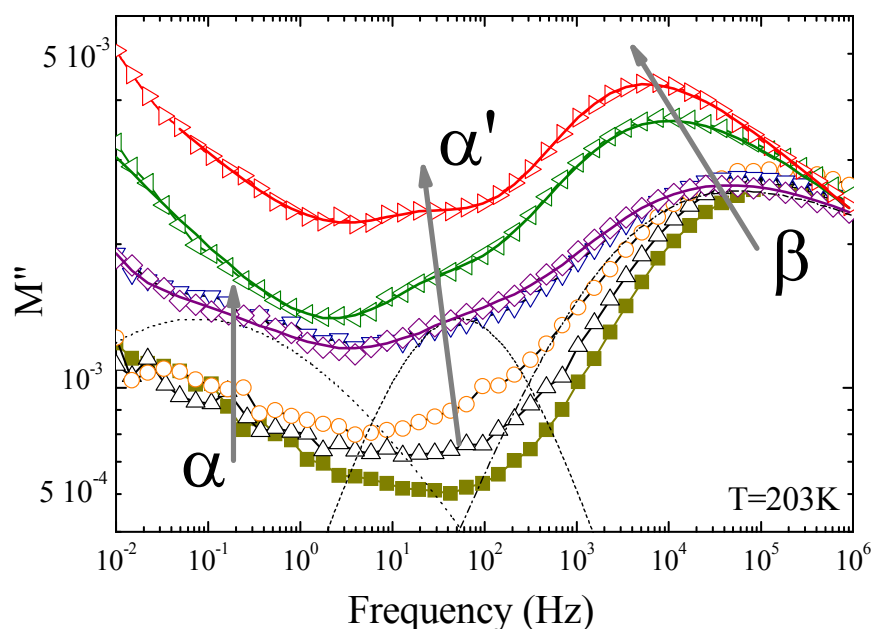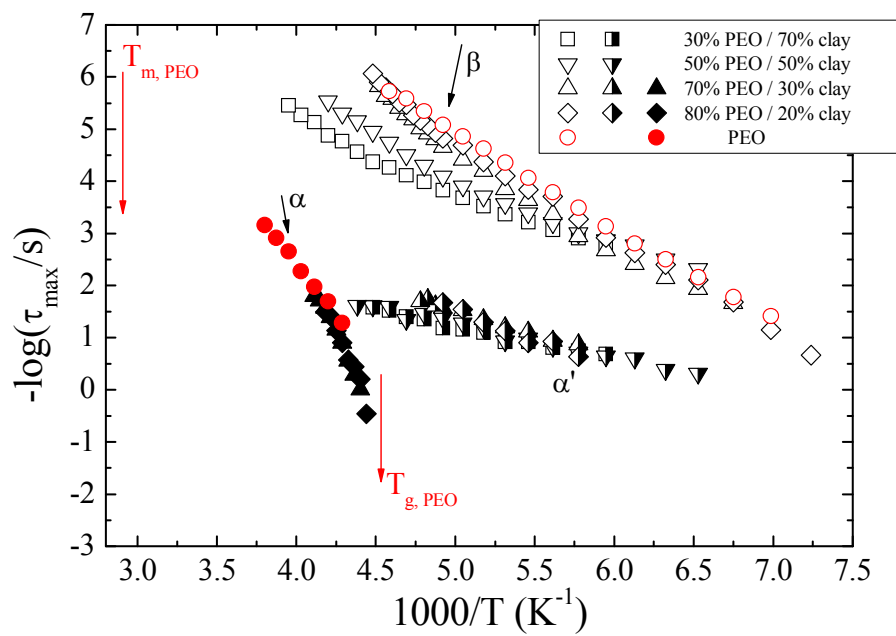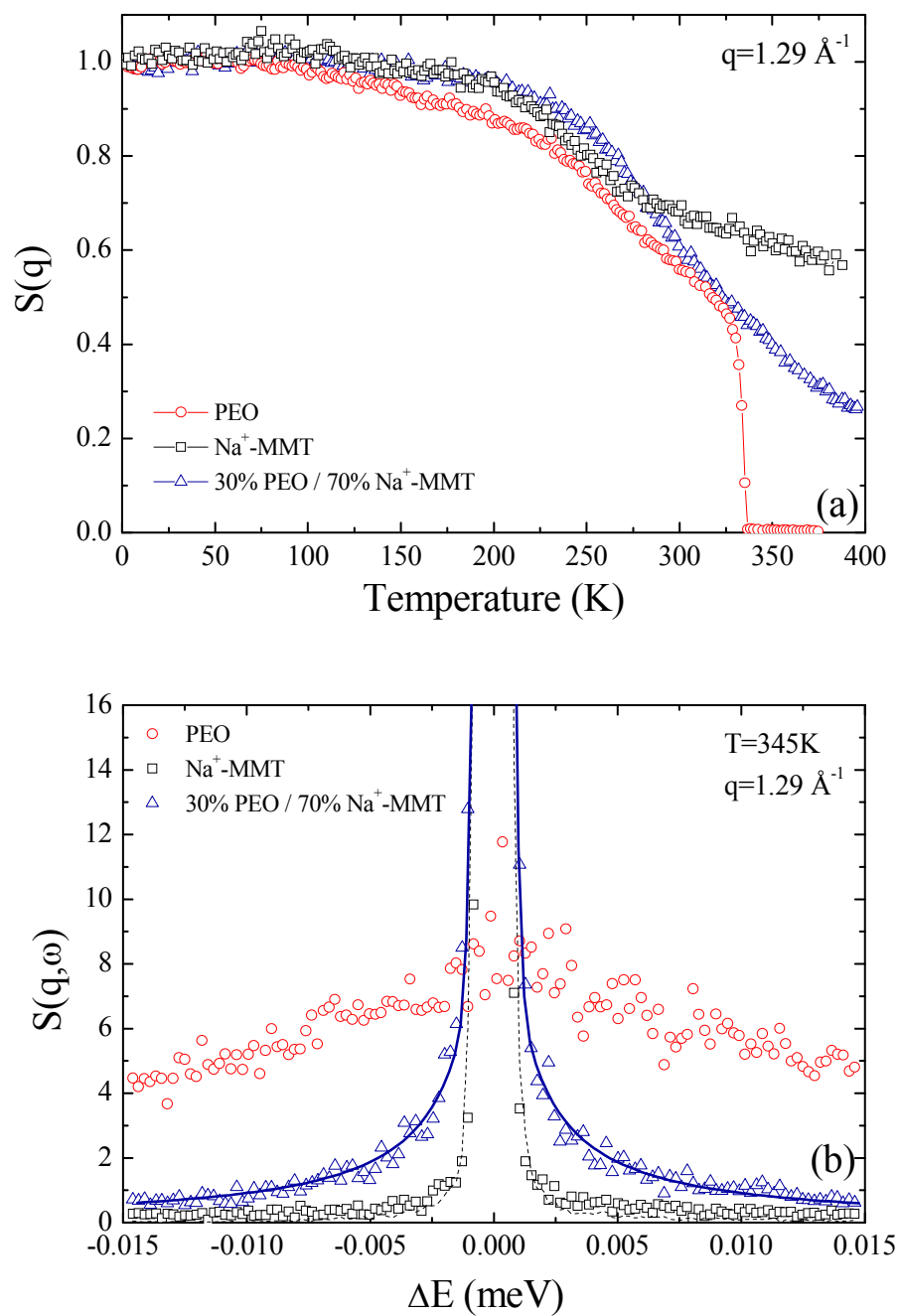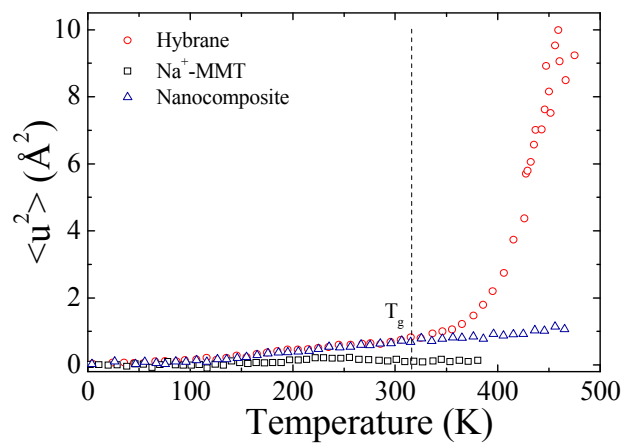
Soft Matter
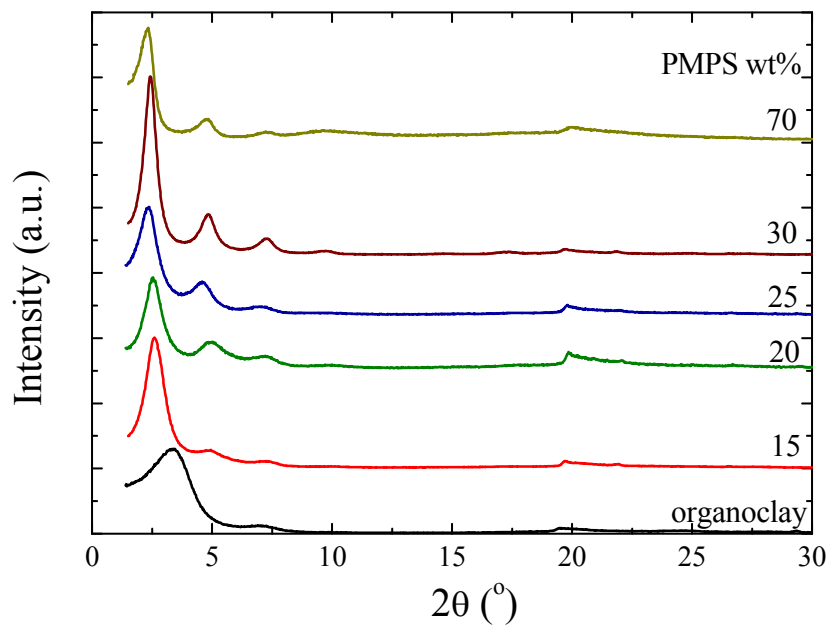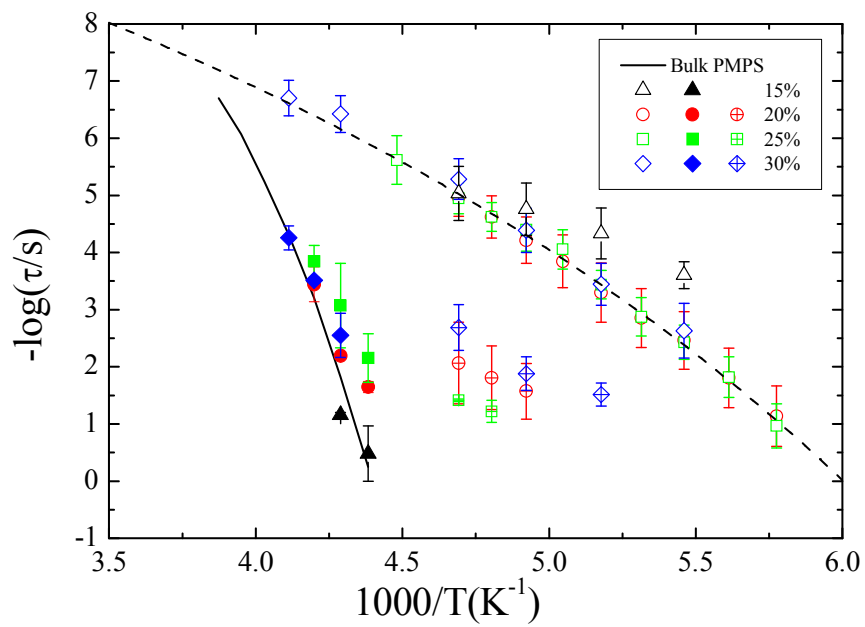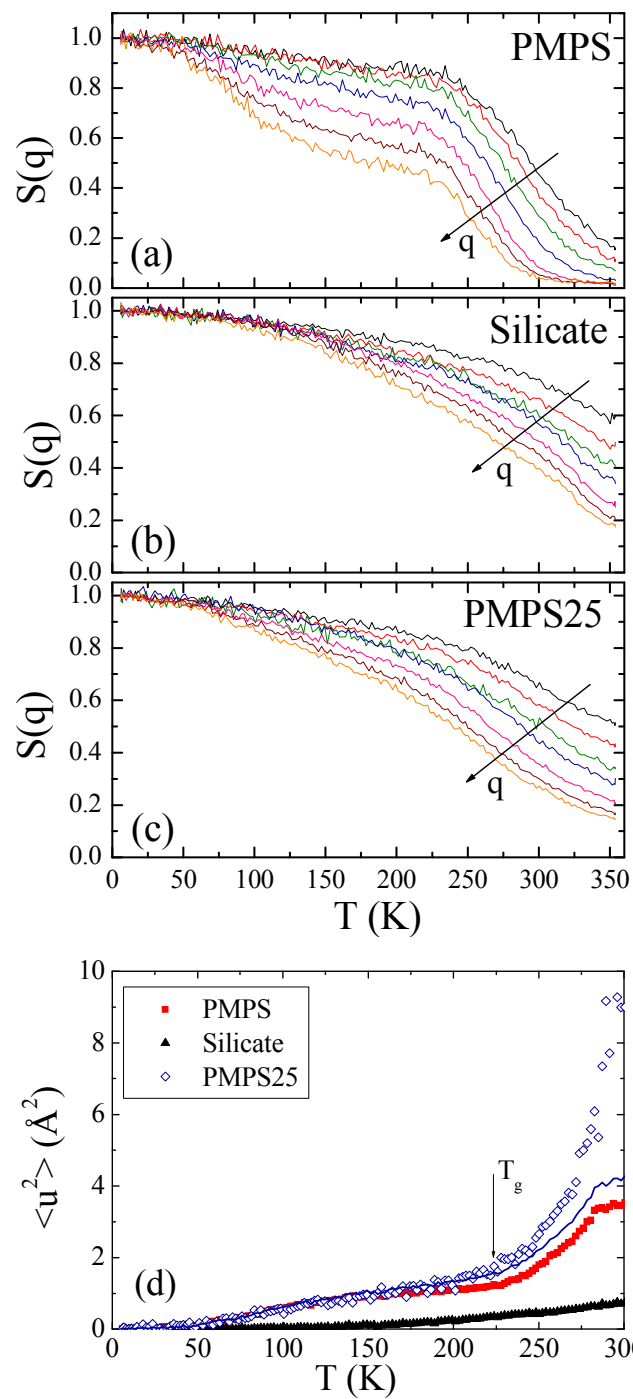
Figure 1

Figure 2

Figure 3

Figure 4

Figure 5

48

Figure 6

Figure 7

50
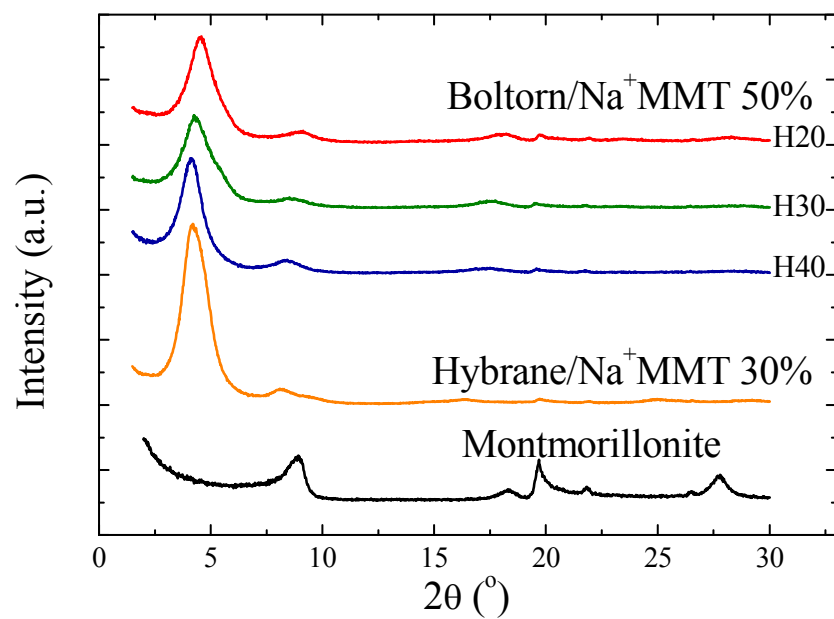
Figure 8

Figure 9

Figure 10
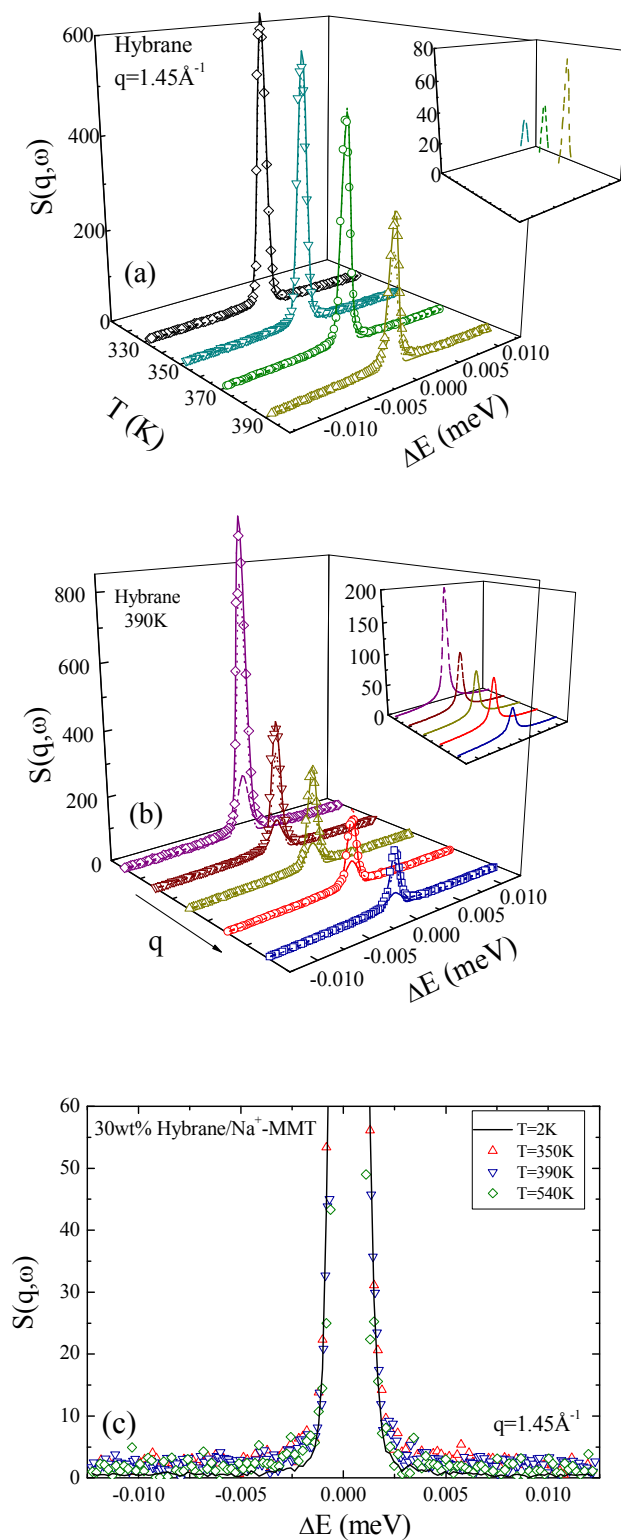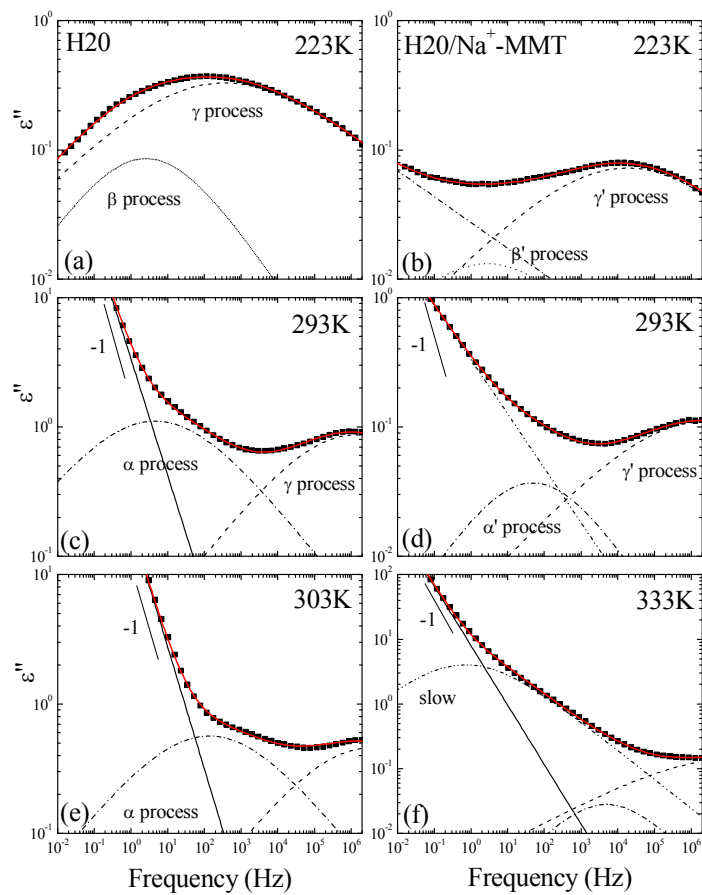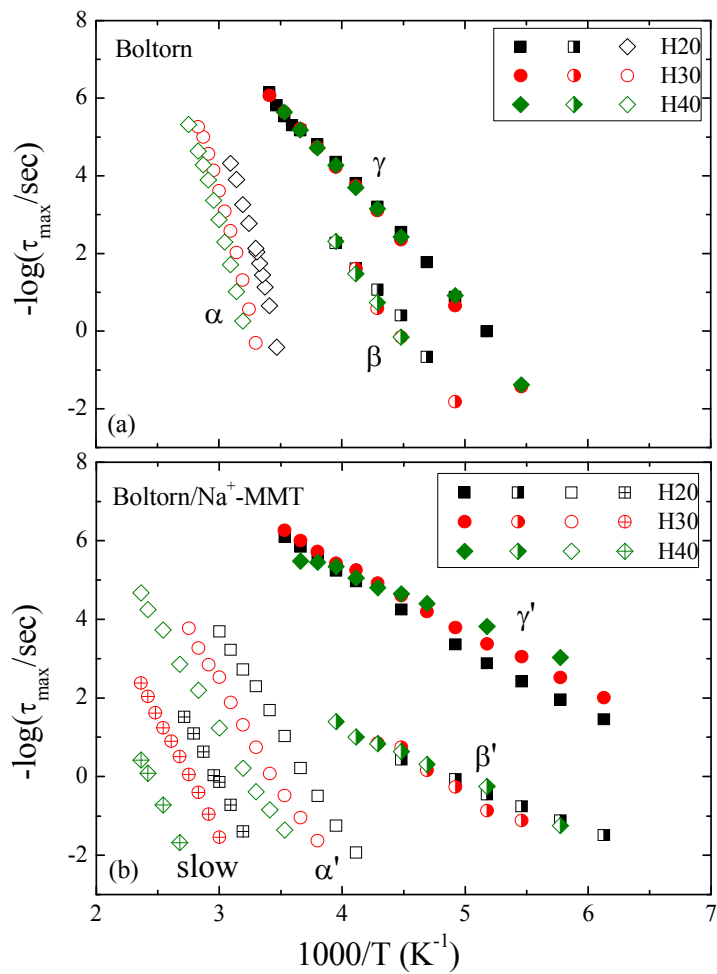
Figure 11

Figure 12

55
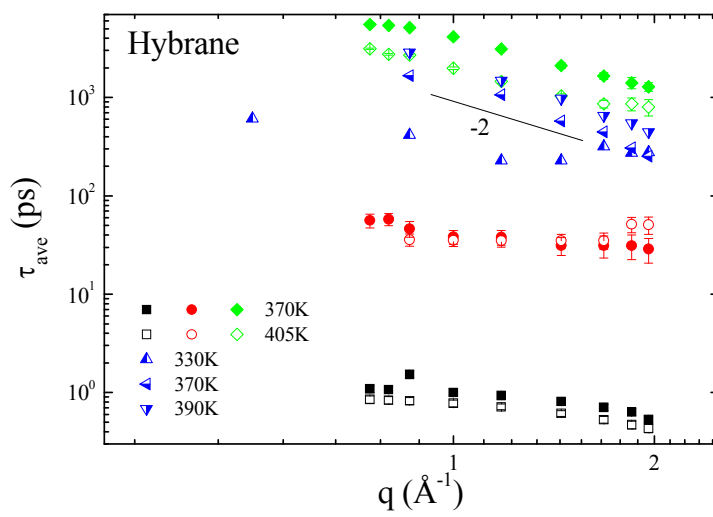
Figure 13

Figure 14

For Table of Contents Use Only

"Effects of Nanoscopic-Confinement on Polymer Dynamics"

K. Chrissopoulou and S. H. Anastasiadis